Review

Carbon Nanohorns and Their Nanohybrid / Nanocomposites as Sensing Layers for Chemoresistive RH Sensors – a Review

Bogdan-Catalin Serban *, Octavian Buiu, Marius Bumbac *, Niculae Dumbrăvescu, Mihai Brezeanu, Matei Gabriel Ursachescu, Vlad Diaconescu, Maria Ruxandra Sălăgean, Cornel Cobianu

Posted Date: 16 July 2025

doi: 10.20944/preprints202507.1413.v1

Keywords: carbon nanohorns; resistive sensors; hydrophilic polymers; nanocomposites; monohybrids

Review

Carbon Nanohorns and Their Nanohybrid/Nanocomposites as Sensing Layers for Chemoresistive RH Sensors - A Review

Bogdan-Catalin Serban [1,*], Octavian Buiu [1], Marius Bumbac [2,*], Niculae Dumbrăvescu [1], Mihai Brezeanu [3], Ursăchescu Matei-Gabriel [4], Vlad Diaconescu [5], Maria Ruxandra Sălăgean [6] and Cornel Cobianu [7,8]

[1] National Institute for Research and Development in Microtechnologies, IMT-Bucharest, Str. Erou Iancu Nicolae 126A, 077190 Voluntari, Romania

[2] Sciences and Advanced Technologies Department, Faculty of Sciences and Arts, Valahia University of Târgoviște, Aleea Sinaia 13, 130004, Târgoviște, Romania

[3] Faculty of Electronics, Telecommunications, and IT, National University of Science and Technology Politehnica Bucharest, Bd Iuliu Maniu 1-3, 061071 Bucharest, Romania

[4] National College "B. P. Hasdeu", Bulevardul Gării, 1, Buzău, 120018, Romania

[5] Faculty of Medicine, University of Medicine and Pharmacy "Carol Davila", Dionisie Lupu Street, No. 37, Sector 2, 030167 Bucharest, Romania

[6] National College "Saint Sava", 23 General H. M. Berthelot Street, Bucharest, Romania

[7] Academy of Romanian Scientists (ARS), Str. Ilfov Nr. 3, Sector 5, Bucharest, Romania

[8] eBio-hub Center of Excellence in Bioengineering, National University of Science and Technology Politehnica Bucharest, Romania

* Correspondence: bogdan.serban@imt.ro (B.-C.S.); Tel.: +40-724284128 (B.-C.S.); marius.bumbac@valahia.ro (M.B.); Tel.: +40-721219270 (M.B.)

Abstract

Carbon nanohorns (CNHs), their nanocomposites, and nanohybrids have demonstrated significant potential for relative humidity (RH) monitoring at room temperature (RT) due to their exceptional physicochemical and electronic properties. At the same time, over the last few decades, resistive sensors have been extensively designed and manufactured due to their simple design, small size, low cost, robustness, quick response times, and wide RH measurement ranges. Recently, resistive sensors with CNHs as key sensing elements have been reported for use in RH monitoring. We summarize in this review the recent progress on resistive RT RH sensors based on CNHs. The most effective strategies to synthesize CNHs and approaches for functionalization, as well as the most relevant physicochemical and electronic properties of nanohorns, are presented in the first two sections of this review. The design of various RH resistive sensors, employing carbon nanohorn-based materials as sensing films, and the synthesis and performance of several CNH-based sensing materials in RH monitoring within the context of resistive sensor design are presented in the following two parts of this review. Pristine and functionalized carbon nanohorns, nanocomposites with different hydrophilic polymers, and nanohybrids with several semiconducting metal oxides are compared in terms of sensitivity, response time, and recovery time. The fifth part of this review presents several sensing mechanisms that are involved in RH monitoring. Finally, in the sixth part of this review, the authors aim to explain which are the most important advantages of using CNHs- based sensing layers in resistive RH detection and why these nanocarbonic materials are less used, at least for the moment, than graphene, graphene oxide, reduced graphene oxide, single and double- walled carbon nanotubes.

Keywords: carbon nanohorns; resistive sensors; hydrophilic polymers; nanocomposites; monohybrids

 doi:10.20944/preprints202507.1413.v1

1. Introduction

Relative humidity (RH), a key environmental parameter that significantly impacts all life forms, is defined as the ratio of the amount of water vapor in the air relative to the amount of water vapor the air can hold at a specific temperature [1]. The RH level affects human ability to regulate body temperature, influences the growth of harmful microorganisms, and can impact the quality of indoor and outdoor environments. Exposure to high RH levels can lead to discomfort, trigger respiratory issues such as bronchoconstriction, and increase the risk of heat-related illnesses. On the contrary, low RH can promote dryness of the skin, a dry throat, irritated eyes, and constricted respiratory passages [2–4]. Monitoring RH is crucial in various commercial, industrial, and residential applications, some of which are depicted in Figure 1 [5–8].

Figure 1. Several application areas for humidity sensors.

Given the above, numerous principles and technologies have been developed over time for performing RH monitoring. The need for accurate and reliable RH measurements has driven innovation in sensor technology, resulting in improvements in range response, linearity, response time, drift, cost-effectiveness, accuracy, and other key metrics [9]. Among the types of sensors used so far in RH monitoring, such as capacitive [10], thermal conductivity [11], magnetoelastic [12], electrochemical [13], surface acoustic wave [14], bulk acoustic wave [15], and optical [16], the resistive sensors are an attractive option [17]. Simple design, small size, low cost, robustness, quick response times, and wide measurement ranges are just some of the advantages that resistive sensors offer in RH monitoring.

The nature of the sensing layer, a key element of a resistive RH sensor, plays a crucial role in manufacturing a resistive device with optimal performance. Consequently, a wide range of materials have been tested as sensing layer within the design of resistive RH sensors: conducting polymers,

 doi:10.20944/preprints202507.1413.v1

such as polypyrrole [18], dielectric polymers, such as polyimide [19], semiconductors, such as cadmium sulfide [20], ZnO [21], SnO2 [22], polyelectrolytes [23], perovskites [24] and so forth.

Carbonic materials were also widely reported as sensing films in the manufacture of RH sensors. Over the last few decades, these materials have gained popularity due to their outstanding properties: high chemical and thermal stability, versatile covalent functionalization to optimize the surface for proper interaction with water molecules, fast charge transfer, a large surface area, low cost, and facile and scalable synthesis [25]. Several carbon-based materials and their nanohybrids/nanocomposites used as sensing elements in the design of RH resistive sensors are listed in Table 1.

Table 1. Examples of nanocarbon-based sensing layers used as sensing elements in the design of RH resistive sensors.

Type of nanocarbonic material	Substrate	Measured RH range (%)	Reference
Graphene	Si/SiO_2	1-96	[26]
Graphene / ZnO	Glass	15- 86	[27]
Graphene / Poly(3,4-ethylenedioxythiophene)- polystyrene sulfonate	Si/SiO_2, Kapton, PET, Paper	30- 95	[28]
Graphene oxide (GO)	Si/SiO_2	40-88	[29]
Reduced graphene oxide / Poly (diallyldimethylammonium chloride) (PDAC)	Glass	20- 70	[30]
Multi-walled carbon nanotubes (MWCNTs)	Polyimide	10- 90	[31]
MWCNTs / Polyvinylpyrrolidone (PVP)	Quartz	11- 94	[32]
Pristine carbon nano-onions (CNOs) / PVP at 1/1 w/w ratio	Polyimide	0-100	[33]
Pristine CNOs / Polyvinyl Alcohol (PVA) at a 1/1 and 2/1 w/w ratios	Si/SiO_2	5-95	[34]
MWCNTs / Polyimide	Si_3N_4	10-95	[35]
Hydrogenated amorphous carbon	Synthetic resin FR2	10-100	[36]
Carbon-black / PVA	glass	10,9 -73,7	[37]
Shellac-derived carbon (SDC)	Si/SiO_2	10-90	[38]
Carbon nano coils (CNCs)	Liquid crystal polymer (LCP)	4-95	[39]
Porous carbon nanofiber	Cellulose	13-97,3	[40]
Carbon nanosheets and nanohoneycombs	Si (100)	11-95	[41]
Carbon quantum dots	Glass sheet	7-95	[42]
Pyrolyzed bamboo	α - alumina	0-96	[43]
Biochar	α-alumina	5-100	[44]
Graphene quantum dots	Si/SiO_2	15-80	[45]
Multi-walled carbon nanotubes (SWCNT) / Pt / P_2O_5	Ceramic	1-90	[46]
SWCNTs / PVA filaments	Textile cloth	60-100	[47]
Chitosan / ZnO / SWCNTs	Polyimide	11-97	[48]
Carbon nanodots	Polytetrafluoroethylene (PTFE)	11-94	[49]

 doi:10.20944/preprints202507.1413.v1

In recent years, carbon nanohorns (CNHs) and their nanocomposites or nanohybrids have also gained significant attention as potential materials for gas sensing applications due to their outstanding properties and potential for enhancing gas detection performance [50,51].

This review article focuses on the latest advancements and new perspectives of CNHs (pristine and functionalized), including nanocomposites and nanohybrids, as sensing materials for RH monitoring using resistive sensors. The review is organized into six main parts. In the first part, the main approaches to synthesizing CNHs are described. Significant attention will be devoted to the functionalization of these nanocarbonic structures to optimize their sensing properties towards water molecules. The second part primarily focuses on the most relevant physicochemical and electronic properties of CNHs, which make them valuable sensing materials for RH monitoring. The third part briefly presents the design of the RH resistive sensors, which employ CNHs-based materials as sensing films. The fourth part includes the synthesis and performance of several CNHs-based sensors for RH monitoring within the design of resistive sensors. Thus, pristine and functionalized CNHs, nanocomposites with several hydrophilic polymers, and nanohybrids with several semiconducting metal oxides are analyzed and compared in terms of sensitivity, response time, and recovery time. The fifth part of this review presents several sensing mechanisms involved in RH detection, as well as an analysis of how the properties of each component in the nanocomposite/nanohybrid and the mutual interaction between them influence the discussed RH sensing mechanisms. Finally, in the sixth part of this review, possible opportunities and future research directions are presented. Ultimately, this review seeks to address the question: Is the production of commercial sensors based on CNHs feasible?

2. Structure and Synthesis of Pristine CNHs and Their Derivatives Used in Resistive RH Monitoring

2.1. Structure of CNHs

CNHs (**Figure 2**) are conical carbon nanocages with cone angles of about 20°, constructed from a sp2 carbon sheet of average length from 40 to 50 nm and a diameter range of 2-5 nm [52]. In contrast to carbon nanotubes (CNTs), which are essentially rolled-up graphene sheets, CNHs have a more complex structure that includes a mix of pentagons, hexagons, and heptagons. This structural diversity contributes to their unique chemical properties and potential applications [53].

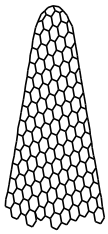

Figure 2. The structure of CNHs.

CNHs tend to aggregate into three distinct structural arrangements: "dahlia-like", "bud-like", and "seed-like". These structures differ in their overall morphology and the arrangement of the individual horn-shaped nanohorns within the aggregate: "dahlia-like resembles a dahlia flower with many petals, "bud-like" resembles a flower bud, and "seed-like" is a more compact arrangement. For many years, this structural characteristic was considered a significant drawback in the functionalization of individual CNHs. However, this limitation has recently been overcome by using a novel technique, recently reported, to separate these supramolecular architectures into individual CNHs [54].

 doi:10.20944/preprints202507.1413.v1

2.2. Synthesis of Pristine CNHs

In the last decades, several approaches to synthesizing pristine CNHs have been developed. All these methods involve the injection of energy to vaporize and rearrange a graphite target, followed by rapid quenching, typically in an inert gas atmosphere. The morphology, size, and purity of CNHs are modulated through variations in various operational parameters, including temperature, current, voltage, and pressure, among others [55].

One of the most commonly used CNHs synthesis routes is that of arc discharge, which involves passing a high current between two graphite electrodes in atmospheric air. The purity of synthesized CNHs is higher than 90% [56]. The arc discharge approach comprises three steps: carbon vaporization, recondensation (where the vaporized carbon atoms recondense as they cool, forming CNHs and other carbon nanomaterials), and purification. The surrounding atmosphere (e.g., air, Ar, CO_2, or CO), gas flow rate, and arc current play a crucial role in determining the type, size, and morphology of the synthesized CNHs [57]. H. Wang et al. [58] reported a cost-effective synthesis of a mixture of 'dahlia-like' and 'bud-like" CNHs based on arc discharge between two graphite rods submerged in liquid nitrogen.

The synthesis of CNHs by CO_2 laser ablation of graphite in the absence of any catalyst was also performed in the last few decades [59]. Synthesis via Joule heating [60] and through inductively coupled plasma [61] represent two other feasible methods for the mass production of CNHs. It is essential to note that the synthesis of CNHs is conducted in the absence of a catalyst, which is a significant advantage compared to, for example, the synthesis of CNTs [54].

2.3. Synthesis of Functionalized CNHs for Resistive RH Monitoring

Due to their predominantly nonpolar carbon structure, pristine CNHs are generally hydrophobic. Therefore, to increase their affinity toward water molecules, their surface must be functionalized to make them more hydrophilic. Oxidation of CNHs with concentrated nitric acid, H_2O_2/hv, or H_2O_2/H_2SO_4 can introduce carboxyl groups onto the surface of the nanocarbonic materials, enhancing their hydrophilicity and dispersibility in polar solvents such as water, isopropanol, and ethanol [62]. Treatments like plasma exposure or oxidation can introduce polar functional groups (like carboxyl or hydroxyl groups) onto the CNHs surface.

The synthesis of oxidized CNHs (CNHox) is carried out using oxygen plasma treatment and water plasma treatment, as depicted in Figure 3. Both types of hydrophilization allow the functionalization of the CNHs by grafting carboxyl, hydroxyl, carbonyl, and epoxy groups. The degree of hydrophilization of the CNHs necessary to achieve superior RH sensing performance (high sensitivity, low response time, low hysteresis, etc.) can be modulated by adjusting the plasma power and exposure time [63].

 doi:10.20944/preprints202507.1413.v1

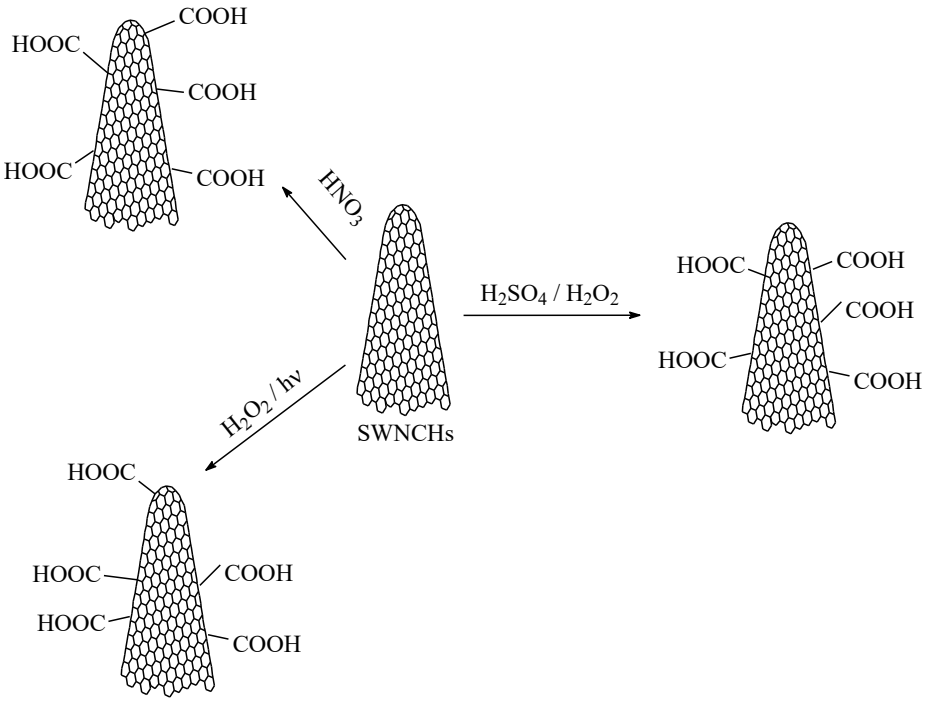

Figure 3. The synthesis of oxidized CNHs (CNHox).

Fluorinated carbon nanohorns (CNHs-F, having the structure presented in **Figure 4**) can also be synthesized and represent a viable option for resistive RH monitoring [64]. The synthesis of CNHs-F is performed by plasma treatment of CNHs in F_2 and N_2 (volume mixture 1:10) at a pressure of 0.5 bar in a nickel reactor at RT. The injection time is 4 minutes, and the exposure time ranges from 2 to 8 minutes.

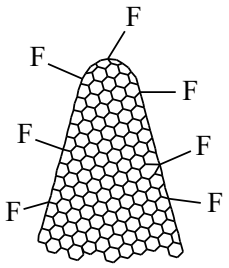

Figure 4. The structure of fluorinated carbon nanohorns (CNHs-F).

Another functionalized carbon nanohorn–based material, oxyfluorinated carbon nanohorns (CNHox-F, with the structure inserted in **Figure 5**), can be synthesized in a two-step plasma procedure [65]. The synthesis of CNHox-F begins by treating CNHs in a volumetric mixture of Ar-O_2 (3:1) in a quartz tube at a pressure of 3 Torr and room temperature (RT). The injection time is 5 minutes, and the exposure time ranges from 2 to 4 minutes. The fluorination of CNHox is carried out by treating ox-CNHs in a F_2 and N_2 plasma (volumetric mixture 1:10) at a pressure of 0.5 bar in a nickel reactor at RT. The injection time is 4 minutes, and the exposure time ranges from 2 to 4 minutes.

The use of CNHox-F as a sensitive layer has several significant advantages. Firstly, the presence of oxygenated functions, generated by treating simple nanocarbon materials with Ar-O_2 plasma, ensures the degree of hydrophilicity necessary for interaction with water. Secondly, due to their increased electronegativity, fluorine atoms enhance the polarity of the nanocarbon material's surface, creating temporary dipoles that facilitate interaction with water molecules.

 doi:10.20944/preprints202507.1413.v1

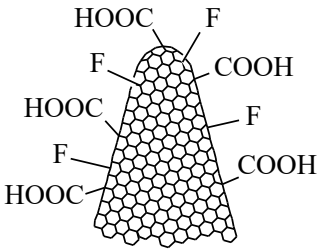

Figure 5. The structure of oxyfluorinated carbon nanohorns (CNHox-F).

3. Properties of CNHs

Due to their unique nanostructure, CNHs exhibit outstanding properties as follows:

- *High thermal conductivity* - The thermal conductivity of CNHs is about 6250 W/m K, larger than that of other nanocarbonic materials, such as CNTs [66,67]
- *High surface area* - CNHs have a large specific surface area, which is a key feature for applications such as catalysis and adsorption [68]
- *Excellent porosity* - The partial oxidation of CNHs gives direct access to internal pores via the generation of nanowindows onto the skeleton of CNHs. Holes can be easily created in pristine CNHs by heat treatment under oxidative and/or acidic conditions [69]
- *High adsorption capacity* - [70]
- *Thermal stability* - CNHs generally exhibit good thermal stability, particularly in inert atmospheres. In air, the oxidation of SWNHs starts above 300°C and is completed at 720°C. CNHs can remain stable in a vacuum up to 1800° C [71]
- *High purity* - CNHs can be synthesized with high purity, often exceeding 95%, and without the need for metal catalysts [72]
- *Chemical stability* - CNHs generally exhibit good corrosion resistance, particularly when compared to some other nanocarbonic materials [73];
- *Low toxicity* - Several experiments conducted in recent years show that CNHs have low toxicity [74]
- *Catalytic properties* - CNHs can act both as catalysts and catalyst supports for metal nanoparticles [75]
- *Good electrical conductivity* - CNHs generally have lower electrical conductivity compared to CNTs; however, the conductivity of both materials can be influenced by several parameters, such as purity, structure, and type of synthesis. The electrical percolation threshold of carbon nanohorns and their derivatives in several hydrophilic polymers is a key parameter in the evaluation of resistive sensing capabilities of nanocomposites based on CNHs for different gases and RH [76,77]
- *Facile covalent and noncovalent functionalization* - [78]

We anticipate that all these features will recommend CNHs as an appropriate substitute for CNTs in the near future.

4. Structure of CNHs-Based Resistive RH Sensors

CNHs-based resistive RH sensors typically include a substrate, a sensing layer, and two metal electrodes. The most used sensing structure (presented in **Figure 6**) is manufactured on a Si substrate (470 μm thick), covered by a SiO2 layer (1 μm thick). The metal stripes of interdigitated transducers (IDT) electrodes typically consist of Cr (10 nm thickness) and Au (100 nm thickness). The width of the electrodes is about 200 μm, with a 6 mm separation between them. The digits of the electrodes have a width and spacing of 10 μm.

 doi:10.20944/preprints202507.1413.v1

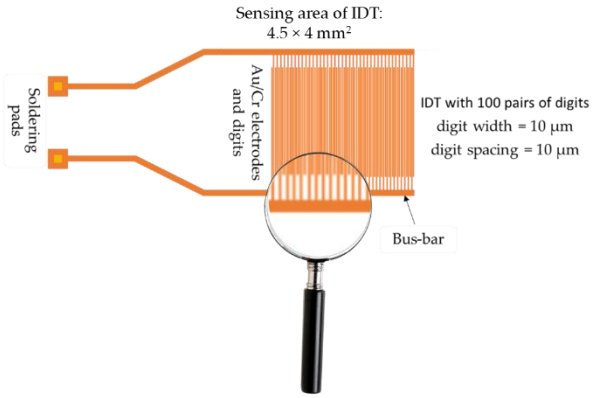

Figure 6. The metal stripes of IDT (Interdigitated structure).

Alternatively, a flexible substrate made from polyimide (3.95 × 3.95 mm²), with gold interdigitated electrodes (Au IDTs), as depicted in Figure 7, can also be used for a CNHs-based resistive RH sensor [76].

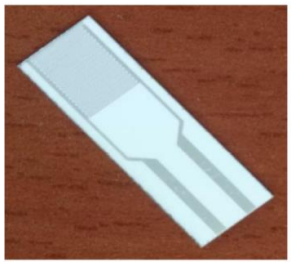

Figure 7. The polyimide-based sensing structure used for resistive RH monitoring.

At the same time, in a simple experimental approach, Selvam et al. [80] have demonstrated the use of cellulose sheet as a flexible substrate. The increase in resistance with the RH level was measured between two nickel electrodes, placed 5 mm apart.

5. RH Resistive Sensors Based on CNHS and Their Nanocomposites/Nanohybrids

The idea of using CNHs and their derivative as a sensing layer within the design of a resistive RH sensor was recently introduced [81]. Oxidized carbon nanohorns (CNHox) – carboxymethylcellulose and CNHox-agarose are the first two carbon nanohorn–based nanocomposites proposed to be used as a sensitive film for resistive monitoring of RH.

5.1 Oxidized CNHs as Sensing Layers in RH Resistive Sensors

Serban et al. used for the first time a sensitive layer based exclusively on a derivative of CNHs, namely CNHox [79,82]. An essential feature of these sensors was the use of a CNHs concentration higher than the percolation threshold in the polymeric matrix, thereby providing lower resistance values. The resistive response of the RH sensor used was investigated by applying a current between the two Cr and Au electrodes deposited on a Si/SiO2 substrate and measuring the resistance when varying the RH from 0% up to 90%, both in humid nitrogen environment (**Figure 8**) and in humid air (**Figure 9**). The resistance of the CNHox-based sensing film increased when the RH increased. The sensor response was compared to that of a commercial sensor (Sensirion® RH sensor).

 doi:10.20944/preprints202507.1413.v1

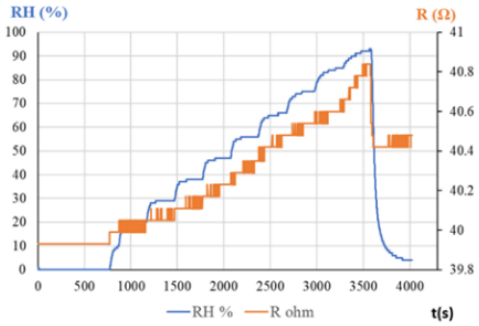

Figure 8. The RH response of the CNHox-based sensor in humid nitrogen (red curve) vs the RH response of the Sensirion RH sensor (blue curve).

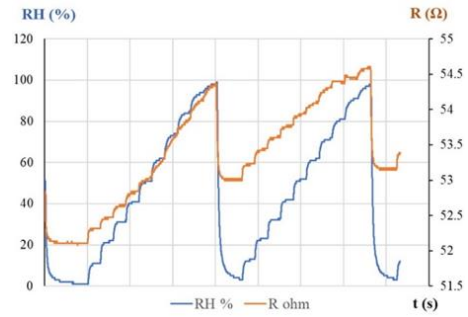

Figure 9. The RH response of the CNHox-based sensor in humid air (red curve) vs the RH response of the Sensirion RH sensor (blue curve).

The manufactured CNHox-based sensor exhibited good linearity in both humid air (R^2 = 0.9844, Figure 10) and humid nitrogen (R^2 = 0.9729, Figure 11).

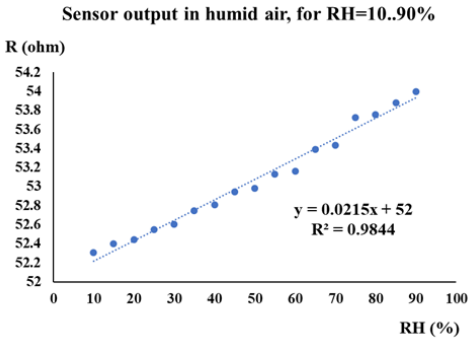

Figure 10. The transfer function of the CNHox-based sensor in humid air (RH = 10% -90%).

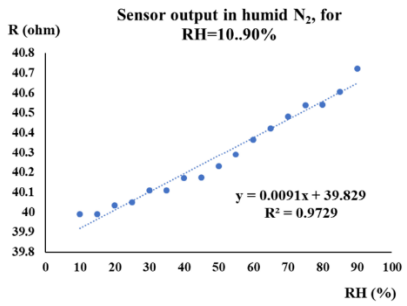

Figure 11. The transfer function of the CNHox-based sensor in humid nitrogen (RH = 10% - 90%).

 doi:10.20944/preprints202507.1413.v1

The sensitivity was approximately 2 times lower in humid nitrogen compared to humid air (9.1 mΩ/RH unit compared to 21 mΩ/RH unit). The response time of the CNHox-based RH sensor in humid nitrogen was 8 seconds, while in humid air, it was 3 seconds.

5.2. Nanocomposite-Based CNHs as Sensing Layers in RH Resistive Sensors

5.2.1. Pristine CNHs–Hydroxyethylcellulose as Sensing Layer in RH Resistive Layers

By combining the appropriate electrical and mechanical properties of pristine CNHs and hydrophilic properties of hydroxyethylcellulose, Selvam et al [80] synthesized a nanocomposite with different loading concentrations of CNHs (5- 50 wt%). The resistance of the nanocomposite was shown to increase with the RH. The response time of the CNHs/cellulose-based sheet was 4 s, while the recovery time was 13 s.

5.2.2 CNHox–PVP as Sensing Layer in RH Resistive Layers

To further improve the sensitivity to water molecules, Serban et al. combined a hydrophilic type of CNH, namely CNHox, with a hydrophilic polymer, namely PVP (the structure is depicted in **Figure 12**), at 1/1 and 2/1 w/w ratios [83], significantly above the percolation threshold of CNHox in PVP. The synthesis of the nanocomposite was shown to be very simple. Initially, both the nanocarbonic material and the PVP were dispersed in deionized water. The CNHox-PVP-deionized water dispersion was further deposited by the drop-casting technique on the IDT structure previously deposited on the Si/SiO_2 substrate to generate the sensing film, in which CNHox and PVP were in a 1/2 w/w/ ratio. The sensing layer was then heated at 80°C for one hour in a vacuum. The sensing capabilities of the manufactured RH detector employing the novel sensing film were explored in a humid nitrogen atmosphere for different RH values and compared with the response of a Sensirion commercial RH sensor (Figure 13). The sensor exhibits a quasi-similar response to that of a commercially available capacitive RH sensor. Experimental data reveal a linear relationship between R and RH for RH < 40%, and a second-order polynomial function variation for RH > 40% in a humid nitrogen atmosphere. The response time of the proposed sensor structure was in the 5.5–5.9 s range.

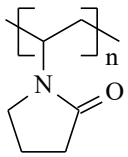

Figure 12. The structure of PVP.

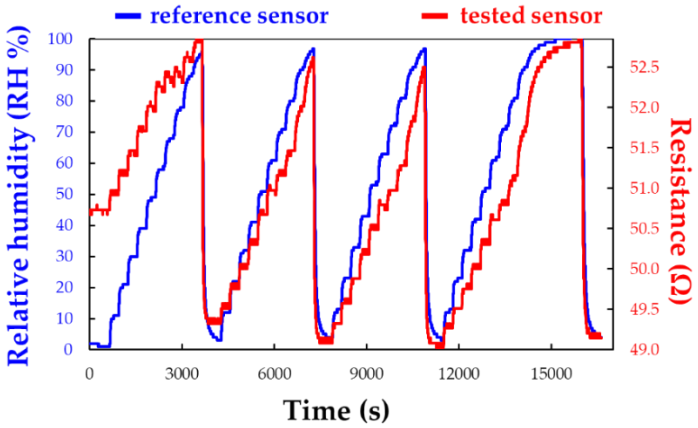

 doi:10.20944/preprints202507.1413.v1

Figure 13. Comparison between the response of the Sensirion commercially available RH sensor (blue line) and the manufactured CNHox-PVP-based (1/2 w/w ratio) RH sensor (red line).

5.2.3. CNHox - poly (ethylene glycol)-blockpoly(propylene glycol)-block-poly (ethylene glycol) (PEG-PPG-PEG) as Sensing Layer in RH Resistive Layers

A matrix nanocomposite based on CNHox and PEG-PPG-PEG (the structure of which is depicted in **Figure 14**) was reported as a sensing layer in the resistive monitoring of RH [83]. In the synthesis process, CNHox and PEG-PPG-PEG (1/6 w/w ratio) were dispersed in deionized water, subjected to magnetic stirring for three hours at RT, and spin-coated on a Si/SiO_2 substrate. The RH detection experiments were conducted by applying a current between the two electrodes: Cr with a 10 nm thickness and Au with a 100 nm thickness. The electrode width was approximately 200 mm, with 6 mm of separation between them, and measuring the voltage difference when varying RH from 0% to 98% (a constant current of 0.1 A was passed through the sensing device). As presented in **Figure 15**, for RH < 60%, the voltage had a relatively low increase with RH, while for RH > 70%, the sensing device exhibited a stronger RH sensitivity. For the entire RH domain, the electrical resistance of the sensing film increases with RH.

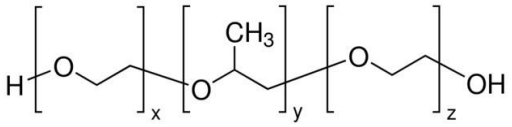

Figure 14. The structure of PEG-PPG-PEG.

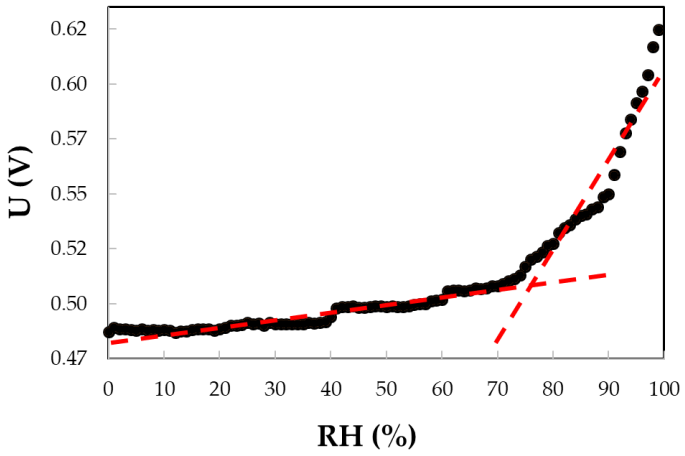

Figure 15. The output signal (voltage) measured when a constant current (0.1 A) is applied to the IDT RH sensing structure, employing the PEG-PPG-PEG nanocomposite as the sensing layer, for variations in RH from 0% to 98%.

5.2.4. GO-CNHox–PVP as Sensing Layer in RH Resistive Layers

A matrix nanocomposite based on GO (the structure is depicted in **Figure 16**), CNHox, and PVP at mass ratios of 1/1/1, 1/2/1, and 1/3/1 w/w/w was recently reported as the sensing layer within the design of RH resistive sensors [84,85]. PVP is a well-known binder, while GO disperses CNHox, increasing the specific surface area of the RH-sensitive layer. The synthesis of the ternary nanocomposite was conducted in an ultrasonic bath using isopropanol. At the end of the synthesis process, annealing of the sensing film was achieved using a two–step procedure: a thermal treatment at 353 K and 2 mbar for 20 hours, followed by a thermal treatment at 383 K and 2 mbar for 90 hours.

 doi:10.20944/preprints202507.1413.v1

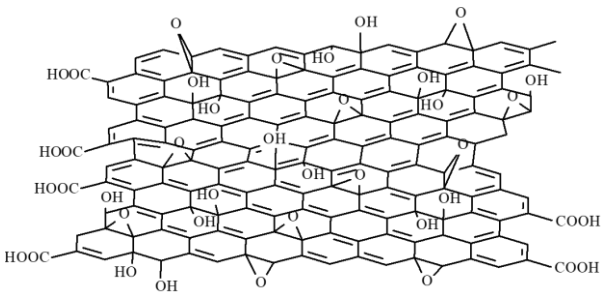

Figure 16. The structure of GO.

Scanning electron micrographs (SEM) of the GO-CNHox-PVP RH sensing film deposited onto the Si/SiO_2 substrate reveal a homogeneous surface, as depicted in **Figure 17**. Multiple mutual interactions between CNHox, GO, and PVP (shown in Figure 18), such as hydrogen bonds, hydrophobic interactions, and π-π interactions, create a supramolecular aggregate that is the key element of the RH monitoring process.

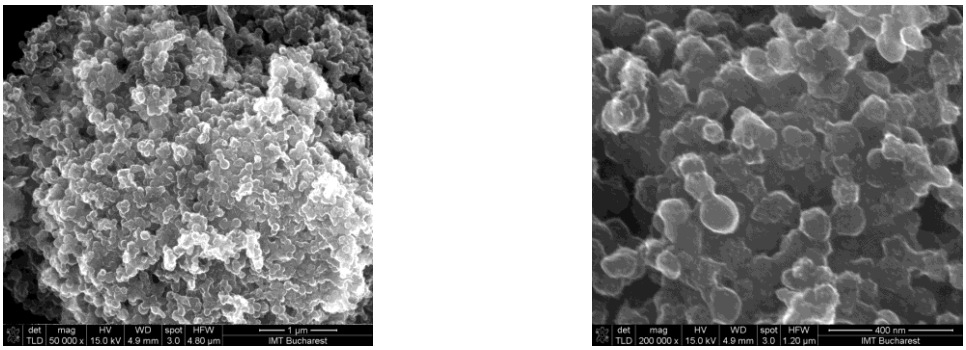

(a) (b)

Figure 17. SEM of the GO–CNHox–PVP–based sensing layer at 1:1:1 w/w/w ratio: a) x 50,000 magnification; b) x 200,000 magnification.

 doi:10.20944/preprints202507.1413.v1

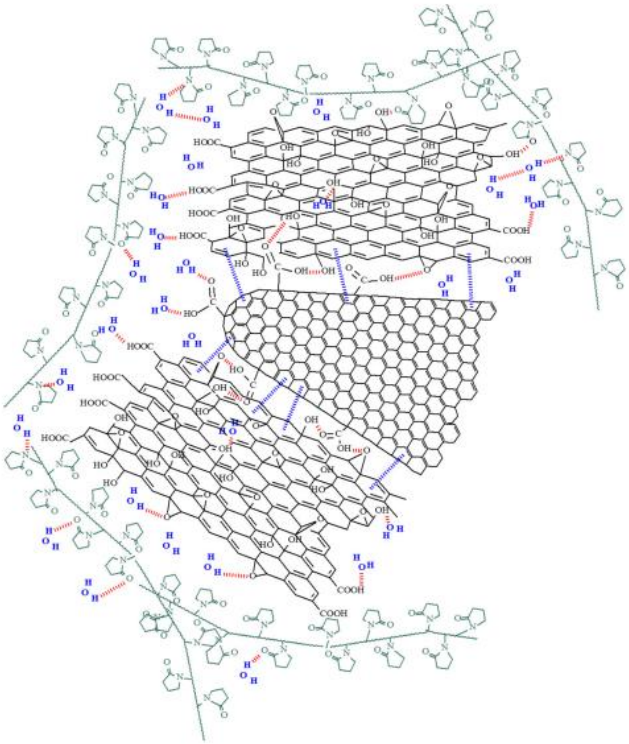

Figure 18. Mutual interactions for the supermolecule generated from CNHox, GO, and PVP.

The linearity of the RH response of the manufactured resistive sensors (sensor 111, sensor 121 and sensor 131 stand for GO-CNHox-PVP at the corresponding 1:1:1, 1:2:1 and 1:3:1 w/w/w mass ratios, respectively), tested in humid nitrogen (for the whole RH range) was shown to be excellent, as depicted in **Figure 19**.

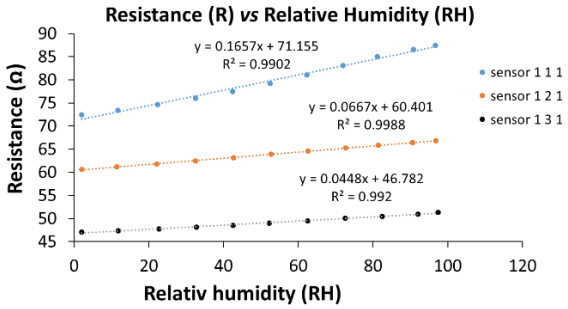

Figure 19. The transfer function of the GO-CNHox-PVP – based (at 1/1/1, 1/2/1, and 1/3/1 w/w/w mass ratios) RH sensors in humid nitrogen (RH = 0%- 100%).

The response and recovery times of sensors 111, 121, and 131 are shown in **Figure 20**. Response time was measured when increasing RH from 40% to 50%, while recovery time was measured when varying RH from 100% to 0% RH. Sensor 111 showed response times in the range of 40–90 seconds, while sensors 121 and 131 had response times between 50–100 seconds and 50–110 seconds, respectively.

 doi:10.20944/preprints202507.1413.v1

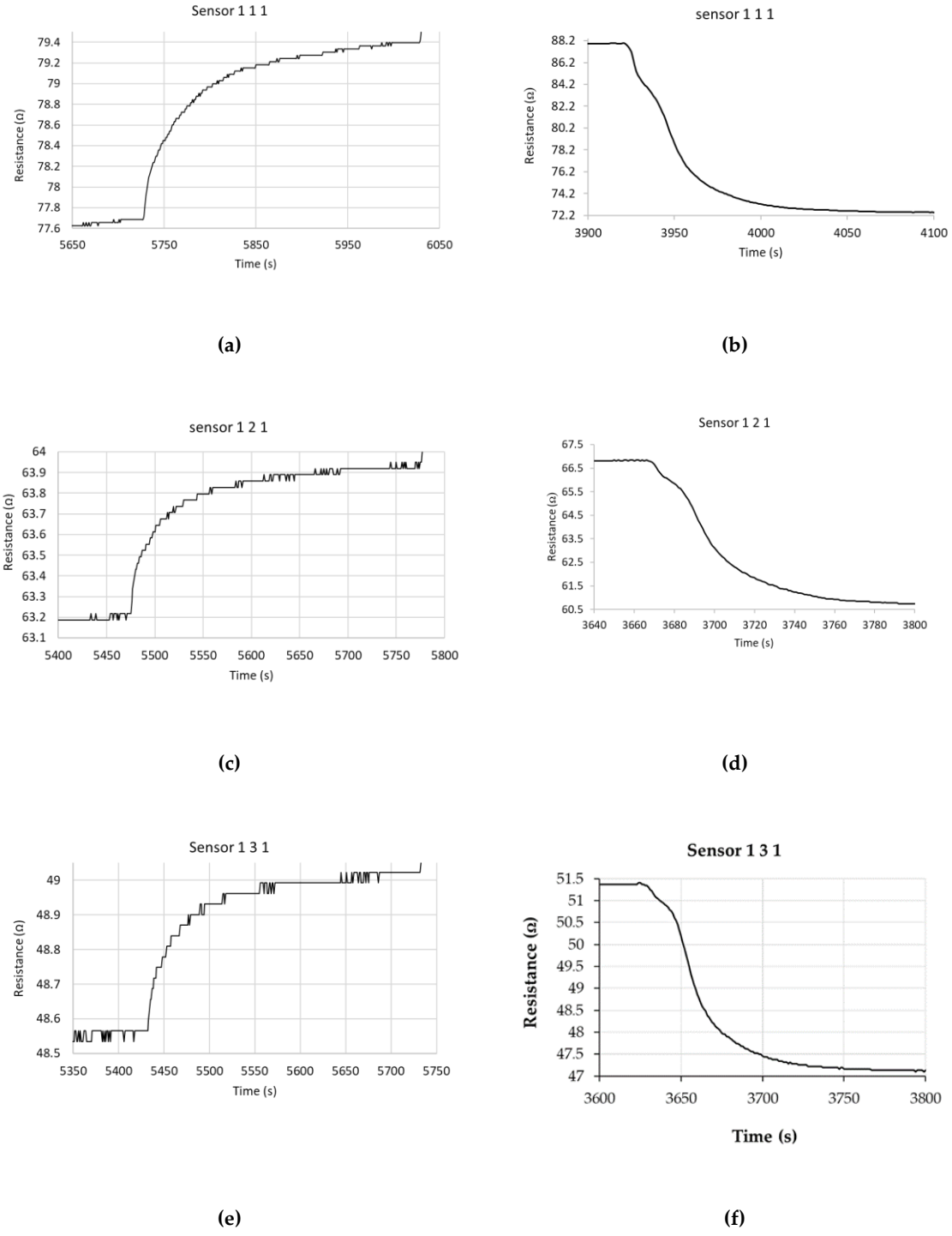

Figure 20. Response and the recovery times of RH sensors 111, 121 and 131 humidity sensors at RT, where (**a**) is response time and (**b**) is recovery time for sensor 111; (**c**) is response time, and (**d**) is recovery time for sensors 121; (**e**) is response time and (**f**) is recovery time for sensor 131. Response time was measured, and RH increased from 40% to 50%. Recovery time was then calculated for RH values varying from 100% to 0%.

The manufactured sensors 111, 121, and 131 had a shorter recovery time compared to the commercial RH sensor when the relative humidity values were decreased from 100% RH to 0% (62 vs 121, 73 vs 111, 73 vs 114).

Upon a simple examination of Table 2, we observe that a sensing film based on CNHox with a hydrophilic polymer, such as PVP, has superior performance in terms of sensitivity compared to the

 doi:10.20944/preprints202507.1413.v1

sensitive layer based on CNHox. Moreover, GO addition has a beneficial effect regarding the sensitivity toward water molecules (Table 2).

Table 2. Comparison of sensitivity for resistive RH monitoring for several sensing layers based on CNHox and their nanocomposites.

Sensing layer composition (w/w)	Substrate	Sensitivity (ΔR/ΔRH)	Reference
CNHox	Si/SiO_2	0.013-0.021	[79]
CNHox/PVP 2/1	Si/SiO_2	0.017-0.025	[83]
CNHox/PVP 1/1	Si/SiO_2	0.020-0.058	[83]
GO/CNHox/PVP 1/3/1	Si/SiO_2	0.043-0.051	[84,85]
GO/CNHox/PVP 1/2/1	Si/SiO_2	0.063-0.070	[84,85]
GO/CNHox/PVP 1/1/1	Si/SiO_2	0.150-0.200	[84,85]

5.2.5. Pristine CNHs-PVP as Sensing Layer in RH Resistive Layers

To optimize the hydrophobic-hydrophilic ratio of CNHs-based sensing layers used in resistive RH sensors, Serban et al. developed a sensing layer based on CNH–PVP at a 9:1 w/w ratio [86,87]. Considering the low solubility of CNHs in water and their hydrophobicity, the nanocomposite was synthesized in dimethylformamide (DMF) using an ultrasonic bath. The CNHs-PVP-DMF dispersion was deposited on a polyimide substrate employing gold electrodes. The CNH-PVP sensing film was annealed for two hours at 100 °C under a vacuum.

The RH detection experimental measurements of the sensor using the CNHs-PVP nanocomposite as the sensing film were conducted by applying a current (0.5- 1 A) and measuring the voltage difference between the electrodes over the entire RH range (0% to 100%). The response of a CNHs–PVP–based manufactured RH sensor was compared to that of a commercial sensor. The resistance of the CNH–PVP–based sensing layer increased when varying RH from 0% to 70%. Once the 70% RH value was reached, the resistance began to decrease with increasing RH. For RH larger than 90%, the resistance started to rise again, as depicted in **Figure 21**. The combination of different sensing mechanisms (decreasing the number of holes in nanocarbonic materials, proton conduction, and swelling of PVP), as well as their relative prevalence, determines the type of response.

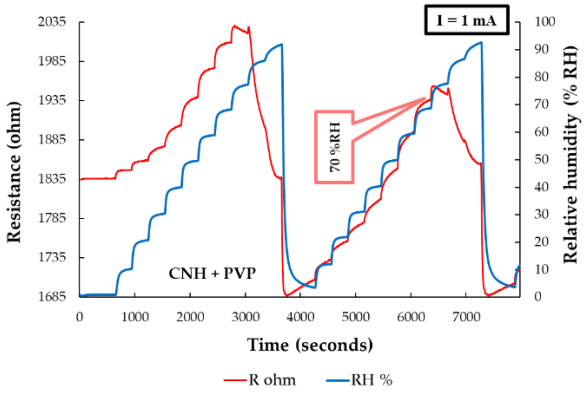

Figure 21. Resistance versus RH variation for the manufactured CNHs–PVP–based sensor (red curve) and the reference commercial sensor (blue curve).

5.3. Organic-Inorganic Nanohybrids Comprising CNHs Used as Sensing Layers in RH Resistive Sensors

Due to the complementary and/or synergetic effects between inorganic and organic components, nanohybrid materials exhibit outstanding properties, such as good mechanical properties, biodegradability, tuned electrical properties, flexibility, enhanced surface area, porosity,

 doi:10.20944/preprints202507.1413.v1

and catalytic properties [88–90]. Therefore, nanohybrids have gained increased interest as a sensing layer in gas detection, with enhanced sensitivity, selectivity, and stability [91]. At the same time, recently, several CNHox-based nanohybrids were reported as sensing layers in resistive RH monitoring, as follows.

5.3.1. Organic-Inorganic CNHox/KCl/PVP Nanohybrids Used as Sensing Layers in RH Resistive Sensors

Several nanohybrids based on CNHox/KCl/PVP, synthesized at mass ratios of 7/1/2, 6.5/1.5/2, and 6/2/2 (w/w/w), were used as sensing films in the design of the resistive RH sensor [92–94]. The associated RH sensors were abbreviated as K1, K2, and K3, respectively. The sensing structure comprised a Si substrate, a SiO_2 layer, and an interdigitated transducer (IDT) based on Cr/Au electrodes. All RH detection measurements, presented in **Figures 22-24**, were conducted by applying a current between the IDTs and measuring the voltage difference as the RH was varied from 0% to 100%. The resistance versus RH behavior of the manufactured sensors, based on CNHox/KCl/PVP as sensing layer, was compared to that of a commercial capacitive RH sensor, used as reference.

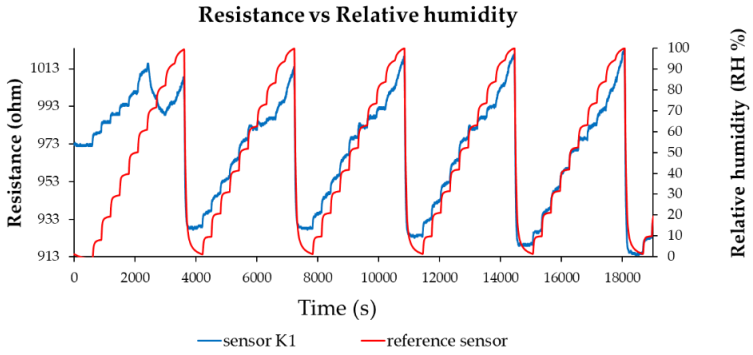

Figure 22. Resistance versus RH for the K1 sensor (employing CNHox/KCl/PVP at a 7/1/2 mass ratio as sensing layer) and for a commercial sensor, used as reference, in several operating sequences.

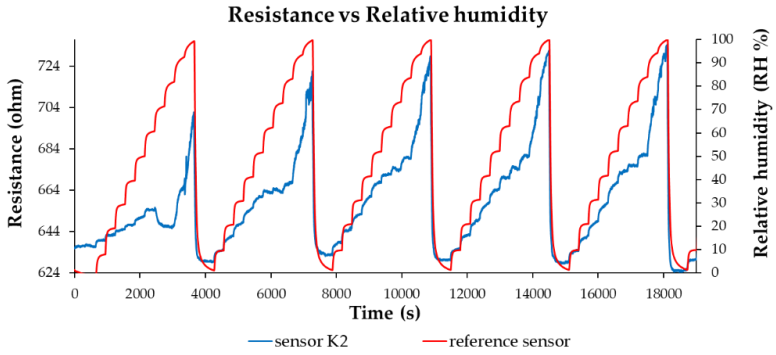

Figure 23. Resistance versus RH for the K1 sensor (employing CNHox/KCl/PVP at 6.5/1.5/2 mass ratio as sensing layer) and for a commercial sensor, used as reference, in several operating sequences.

 doi:10.20944/preprints202507.1413.v1

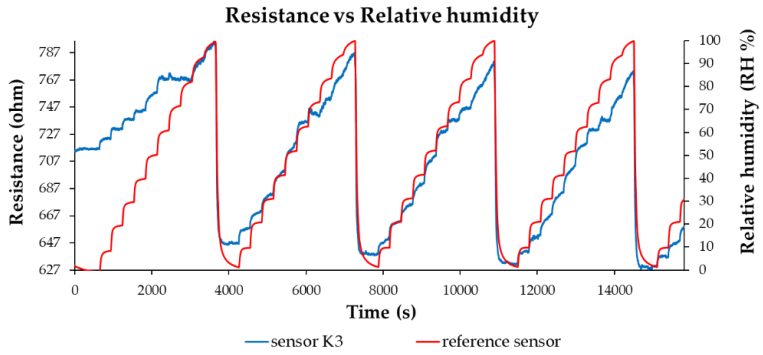

Figure 24. Resistance versus RH for the K1 sensor (employing CNHox/KCl/PVP at a 6/2/2 mass ratio as sensing layer) and for a commercial sensor, used as reference, in several operating sequences.

The manufactured CNHox/KCl/PVP–based sensors, which showed room temperature RH detection behavior comparable to that of the commercial capacitive RH sensor (Fig. 22-24). The devices are characterized by rapid response time (**Figure 25**), good sensitivity, and excellent linearity. For RH < 70%, the commercial sensor has a response time of 60 s ± 10 s, while for RH > 70%, the response time increases to approximately 90 s ± 10 s.

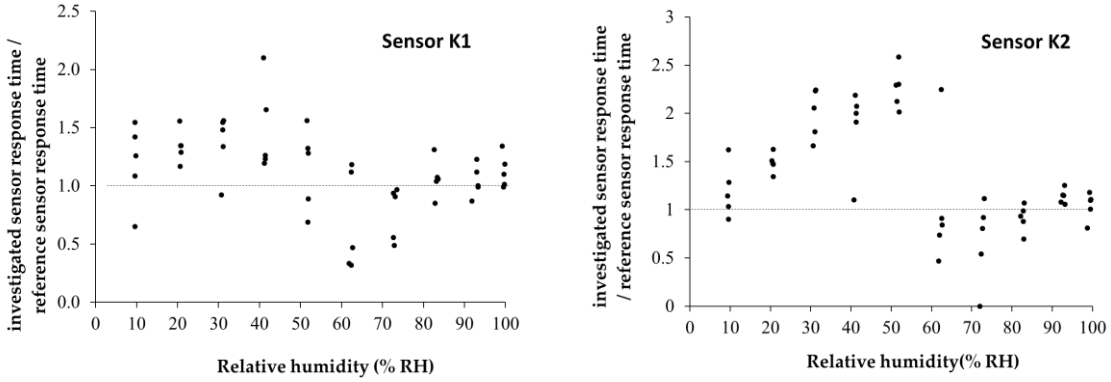

(a) (b)

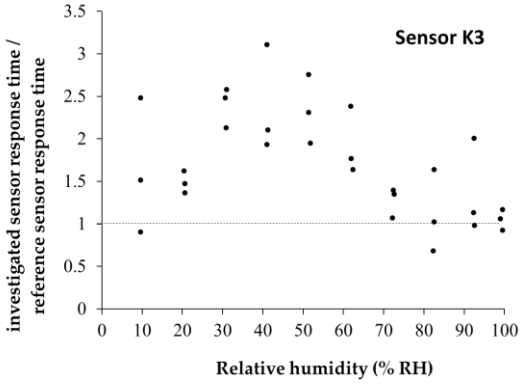

(c)

Figure 25. Graphical representations of the ratios between the response time of the manufactured CNHox/KCl/PVP–based sensors (a) K1 sensor, b) K2 sensor, and c) K3 sensor) and the response time of the commercial sensor, measured in humid nitrogen, when varying RH from 0% to 100%.

 doi:10.20944/preprints202507.1413.v1

5.3.2. Organic-Inorganic CNHox/TiO2/PVP Nanohybrids Used as Sensing Layers in RH Resistive Sensors

Serban et al reported the use of CNHox/TiO_2/PVP nanohybrid as a sensing layer for RH resistive monitoring [95,96]. Three types of CNHox/TiO_2/PVP nanohybrids were synthesized, at 1/1/1 (corresponding to the manufactured sensor T1), 2/1/1 (corresponding to the manufactured sensor T2), and 3/1/1/ (corresponding to the manufactured sensor T3) mass ratios (w/w/w). The synthesis of the nanohybrids was conducted in ethanol using an ultrasonic bath. The mutual interaction between CNHox, titania, and PVP was confirmed using Raman spectroscopy. The Raman spectra for the CNHox/TiO_2/PVP at a 3:1:1 w/w/w mass ratio, deposited on the substrate, recorded at four points of the nanohybrid, are presented in **Figure 26**.

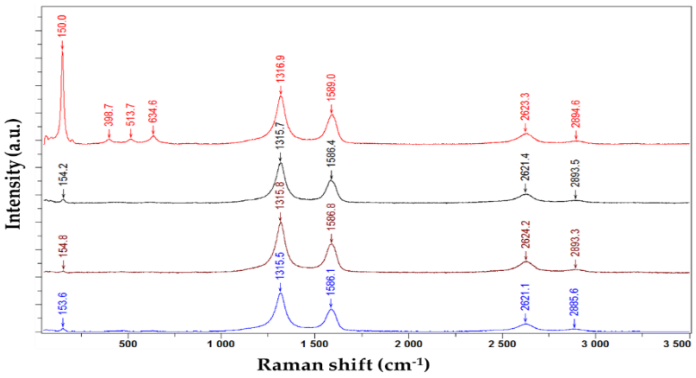

Figure 26. Raman spectra of the CNHox/TiO2/PVP nanocomposite solid-state film, with a 3:1:1 w/w/w mass ratio, deposited on glass, were recorded at four different points of the nanohybrid.

Three active Raman bands (D, G, and 2D) were measured at wavenumbers of 1316.9, 1589, and 2623.3 cm-1, which confirm the presence of CNHox [79,83]. Distinct anatase TiO2 bands, such as Eg1 mode at 150 cm-1, B1g at 398.7 cm-1, A1g at 513,7 cm-1, and Eg3 at 634.6 cm-1, were also recorded [97–99]. The corresponding peaks of PVP are likely hidden, most probably due to being masked by CNHox. The shift in Raman peak positions between individual TiO2 and CNHox and those of the same materials as components of the nanohybrid is a consequence of noncovalent interactions between them, such as hydrogen bonds and electrostatic interactions.

The resistance of the CNHox–TiO2–PVP–based sensing film increases when RH increases from 0% to 80% RH (**Figures 27-29**). For RH larger than 80%, subtle differences are recorded. Thus, the resistance of T1 sensor moderately decreases with increasing RH, while the resistance of manufactured sensors T2 and T3 rises with RH. As shown in **Figures 27-29**, the performance of the manufactured CNHox-TiO_2–PVP-based RH sensors is comparable to that of a commercial RH sensor used as a reference.

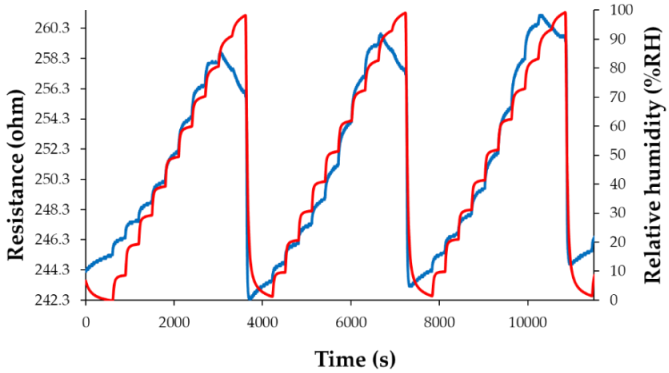

 doi:10.20944/preprints202507.1413.v1

Figure 27. The response of the manufactured sensor T1 (the blue curve) as a function of time for three complete measurement cycles, when varying RH between 0% and 100%; "RH curve-red" shows the variation of the RH in the testing chamber, as indicated by the reference sensor.

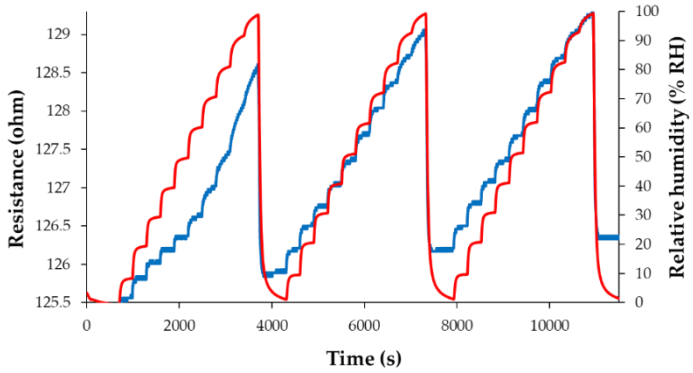

Figure 28. The response of the manufactured sensor T2 (the blue curve) as a function of time for three complete measurement cycles, when varying RH between 0% and 100%; "RH curve-red" shows the variation of the RH in the testing chamber, as indicated by the reference sensor.

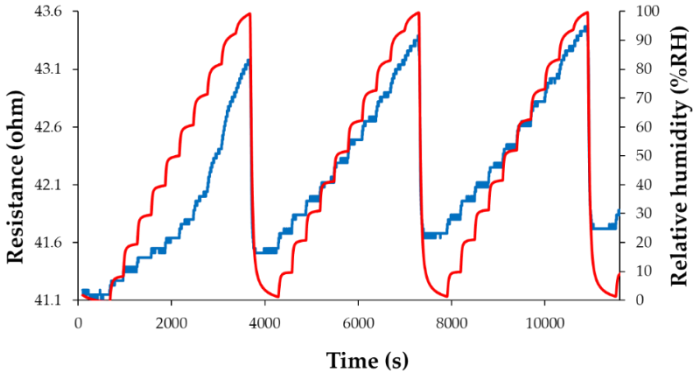

Figure 29. The response of the manufactured sensor T2 (the blue curve) as a function of time for three complete measurement cycles, when varying RH between 0% and 100%; "RH curve-red" shows the variation of the RH in the testing chamber, as indicated by the reference sensor.

5.3.3. Organic-Inorganic CNHox/ZnO/PVP Nanohybrids Used as Sensing Layers in RH Resistive Sensors

Serban et al [100] deposited a ternary nanohybrid based on CNHox, ZnO, and PVP at a 5/2/1 mass ratio on a Si/SiO_2 substrate using the drop casting method. The morphology and composition of the sensing film were evaluated and confirmed through SEM and Raman spectroscopy. Experimental measurements showed that the resistance of the sensitive film increased with RH, varying from 0% to 100%. Increased RH sensitivity was recorded for RH > 60%. The response time of the manufactured CNHox-ZnO-PVP-based RH sensor was shown to be comparable to that of a commercially available capacitive RH sensor.

5.3.4. Organic-Inorganic CNHox/SnO2/ZnO/PVP Nanohybrids Used as Sensing Layers in RH Resistive Sensors

A thin film based on a quaternary nanohybrid comprising CNHox/SnO_2/ZnO/PVP was tested as a sensing layer in the resistive monitoring of RH [101]. Two CNHox/SnO_2/ZnO/PVP–based sensing layers were synthesized and deposited, at 1.5/1/1/1 (abbreviated as "sensor 1.5") and 3/1/1/1 (abbreviated as "sensor 3") mass ratio. The RH sensing device consists of a Si/SiO_2 substrate and interdigitated transducers (IDT) electrodes (Cr/Au). As depicted in **Figure 30**, for both

 doi:10.20944/preprints202507.1413.v1

CNHox/SnO_2/ZnO/PVP nanohybrid-based sensing layers, the resistance increases when RH increases from 0% to 100%. Their experimental performance was compared to that of a commercial RH sensor, used as a reference.

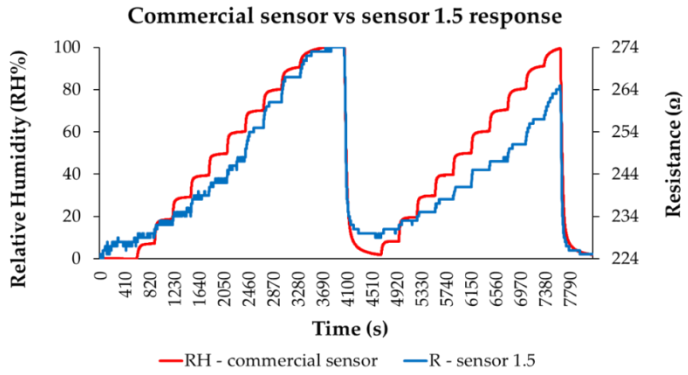

a)

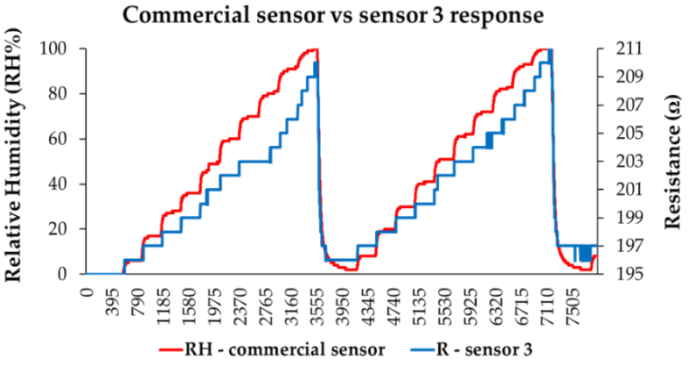

b)

Figure 30. The response of: a) "Sensor 1.5", and b) "Sensor "3" ("R curve"-blue) as a function of time for two measurement cycles, while increasing RH in 10 steps from 0% to 100% RH; "RH curve-red" shows the similar characteristic measured for a commercial, capacitive sensor.

The response time of the CNHox/SnO2/ZnO/PVP–based manufactured RH sensors ranged from 35 to 100 seconds for both devices, as presented in Figure 31. The highest values of response time were recorded at RH > 70%, most likely due to a decrease in the number of active sites.

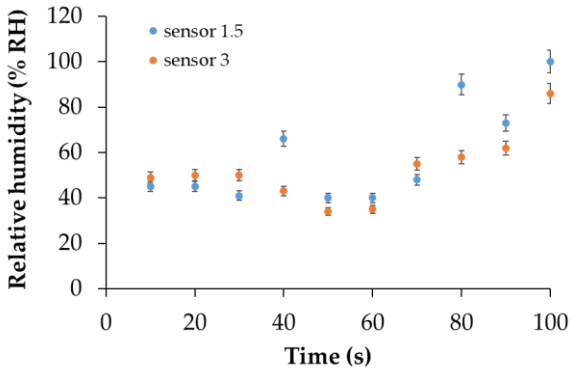

 doi:10.20944/preprints202507.1413.v1

Figure 31. Response times for "Sensor 1.5" and "Sensor 3" with RH increasing from 0% to100%, with a 10% step, in the second measurement cycle.

Figure 32 shows the recovery pattern for both quaternary nanohybrid-based RH sensing layers measured when the RH from the testing box dropped from 100% to 0%. The calculated recovery times varied from 65 s to 100 s, values similar to those exhibited by the commercial sensor, which was employed as a reference.

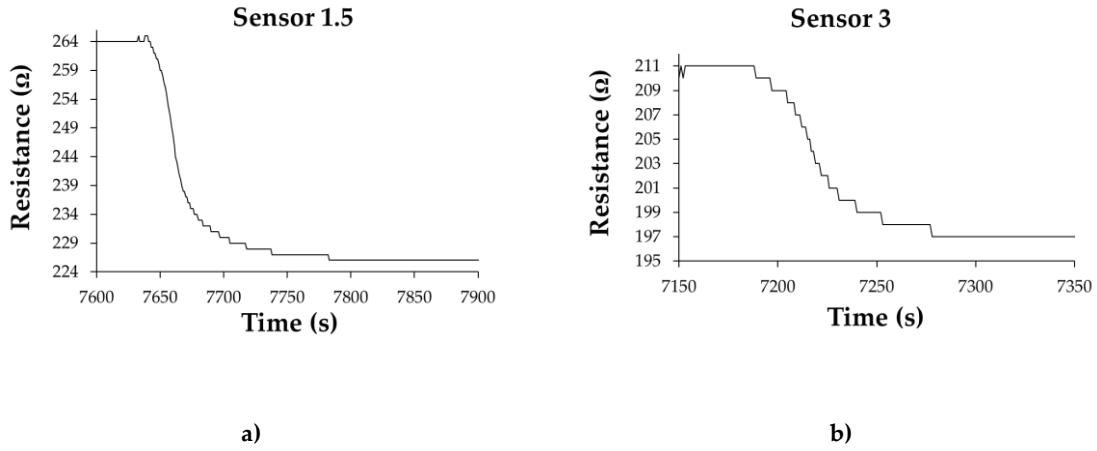

a) **b)**

Figure 32. Recovery times for a) "Sensor 1.5" and b) "Sensor 3" after the second measurement cycle; the recovery time was measured by varying RH from 100% to 0% (clean, dry nitrogen).

5.3.5. Organic-Inorganic CNHox/GO/SnO2/PVP Nanohybrid Used as Sensing Layers in RH Resistive Sensors

Thin films based on a quaternary nanohybrid based on CNHox/GO/SnO2/PVP were also demonstrated as sensing layers in RH resistive sensors [102]. Two CNHox/GO/SnO2/PVP-based sensing layers were synthesized, at 1/1/1/1 (abbreviated as "sensor 1") and 0.75/0.75/1/1 (abbreviated as "sensor 0.75") mass ratios. The RH sensing device consisted of a Si/SiO2 substrate and interdigitated, Cr-Au transducers (IDT) electrodes. The composition and the morphology of the CNHox/GO/SnO2/PVP-based sensing films were explored and confirmed through X-ray diffraction (XRD), Scanning Electron Microscopy (SEM), and RAMAN spectroscopy. As depicted in Figure 33, for both CNHox/GO/SnO2/PVP nanohybrid-based RH sensing layers employed, the resistance increased when varying RH from 0% to 100%. A notable characteristic of these two manufactured CNHox/GO/SnO2/PVP–based sensors is their low power consumption, which is below 2 mW. Their experimental performance was compared to that of a commercial capacitive RH sensor, used as a reference.

 doi:10.20944/preprints202507.1413.v1

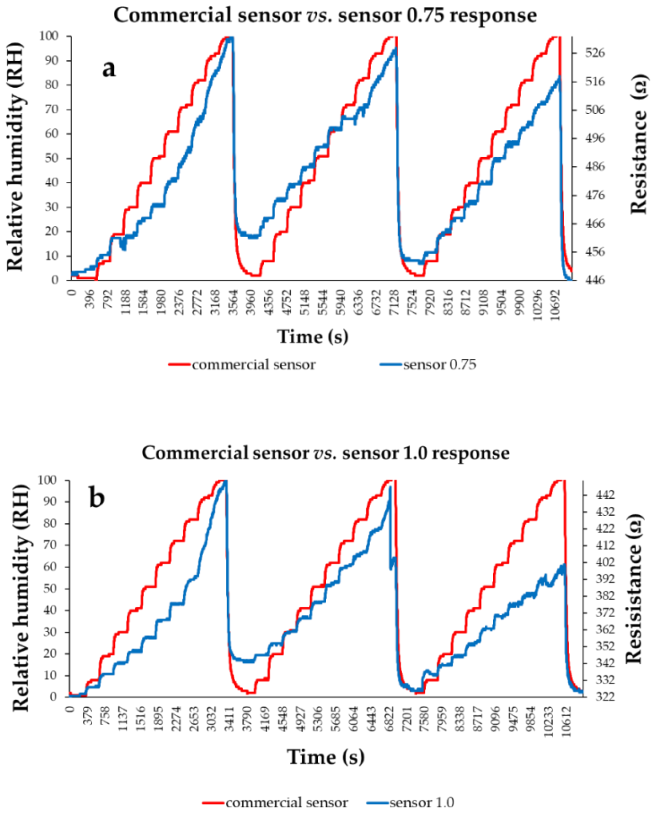

Figure 33. The response of (a) "Sensor 0.75" and (b) "Sensor 1.0" ("R curve-blue" curves) presented as a function of time for three measurement cycles while varying RH, in 10 steps, from 0% to 100%; "RH curve-red" shows the similar characteristic measured for a commercial, capacitive sensor.

The linearity of the manufactured CNHox/GO/SnO2/PVP–based sensors was excellent, as demonstrated by the transfer function shown in Figure 34.

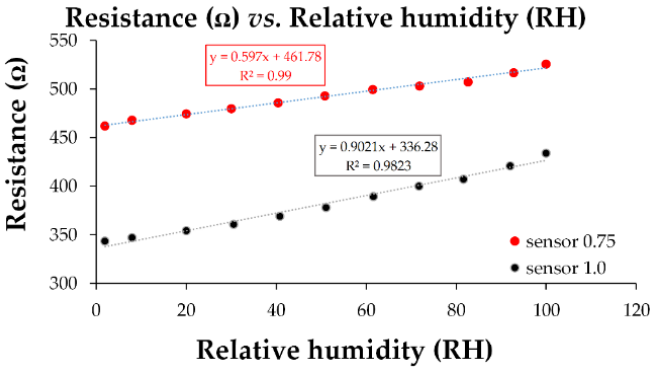

Figure 34. The transfer function of the quaternary CNHox/GO/SnO2/PVP nanohybrid-based resistive sensors in humid nitrogen (RH = 0%–100%).

6. Sensing Mechanisms for RH Resistive Monitoring Using CNHs and Their Nanocomposites/Nanohybrids

Any hypothesis regarding the RH resistive monitoring sensing mechanisms using CNHs (pristine and their derivatives) or nanocomposites/nanohybrids based on these nanocarbonic materials begins with the fact that CNHs are p-type semiconducting materials [103,104]. At the same time, it is to be expected that chemisorbed water molecules on the CNHs surface operate as electron

 doi:10.20944/preprints202507.1413.v1

donors [105]. As the electron density increases, the positive charge concentration in CNHs decreases and, thus, the p-type CNHs-based films become more resistive. This scenario accounts for most of the reported experimental results concerning resistive RH sensors employing CNHs-based sensing layers [76,77,83–87,92–96].

The interaction between water and CNHs (as p-type semiconducting materials) can also be discussed from the perspective of the Hard-Soft Acid-Base (HSAB) theory. This theory, proposed by Ralph Pearson in 1963, operates with Lewis acids and bases: a molecule capable of donating electron pairs acts as a base, while a molecule that acts as an electron acceptor is classified as an acid. Lewis acids and bases can be classified into three types: hard, soft, and borderline [106–109]. According to the HSAB concept, strong bases have a greater affinity for interacting with strong acids, while soft bases preferentially interact with strong acids. In contrast, borderline bases tend to interact with borderline acids. Given the above definitions and rules, due to the electron pairs in the oxygen atom, H_2O is a typical example of a hard base and, consequently, has an affinity to interact with the positive charge carriers (hard acids) in the CNHs. In recent years, the HSAB theory has become a valuable tool for selecting sensitive materials for gas sensing, as well as for explaining specific reaction mechanisms [110–112].

At the same time, hydrogen bonds, as well as the electron-withdrawing effect of the carboxyl group (present in CNHox), have an impact on the hole concentration in the nanocarbonic films and can modulate the RH sensitivity, ultimately affecting the RH sensor response [113].

The second plausible RH sensing mechanism considered for the interpretation of the RH sensing experimental results presented in the previous chapter is the swelling of the hydrophilic polymer employed in the nanohybrids sensing layer in contact with water [76,84–87,92–96,7783]. PVP and PEG-PPG-PEG are dielectric polymers with hydrophilic properties, which swell upon interaction with moisture. The swelling of polymers leads to the displacement of the nanocarbonic particles, increasing the distance between the CNHs and decreasing the electrically percolating pathways, as depicted in **Figure 35**. Consequently, the sensing film resistance increases upon exposure to a higher level of RH because more water molecules move into the bulk of the nanocarbonic film.

PVP swelling is more pronounced at higher levels of RH. The swelling of PEG-PPG-PEG is somewhat different than that of PVP and requires a supplementary explanation. PEG-PPG-PEG is less hydrophilic than PVP, and more water molecules are needed to initiate swelling. For RH < 40%, the resistance of PEG–PPG–PEG–based films exhibits a relatively low increase with RH, while for RH > 65% the sensing layer resistance increases sharply with RH (switch-type behavior).

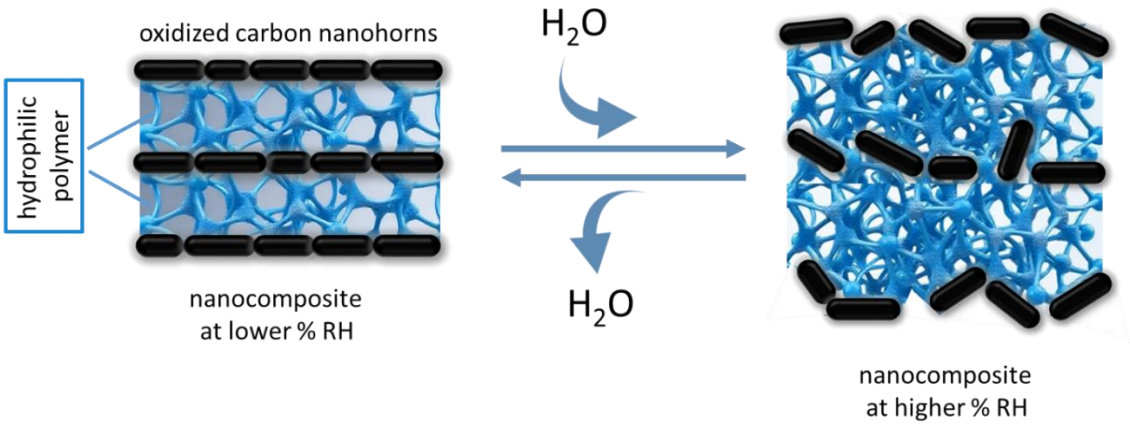

Figure 35. The swelling of the hydrophilic polymer included in CNHs-based nanocomposites upon interaction with water.

A third plausible RH sensing mechanism that needs to be discussed is based on the fact that, given the type of employed analyte (water), protonic conduction must be considered as a potential

 doi:10.20944/preprints202507.1413.v1

contributor to RH sensing. This type of sensing mechanism refers to the dissociation of water (a major contributor) and/or the ionization of carboxylic acids (from CNHox). The adsorbed water molecules on the surface of CNHox may dissociate into H^+ and OH^-. The protons generated by water dissociation and the ionization of carboxylic groups decrease the overall electrical resistance of the sensing layer [114]. However, since the experimental data presented in the previous section show an increase in resistance with RH, one can conclude that the contribution of this third RH sensing mechanism, based on proton tunneling, is relatively small compared to the impact of the first two sensing mechanisms discussed above.

Beyond the three RH sensing mechanisms, the individual contributions of other components in the CNHs-based sensing films, as well as the mutual interactions between them, could also play an essential role in the overall RH sensing mechanism.

7. Why Are CNHs Used Less Frequently than CNTs and Graphene Derivatives for Resistive RH Sensing? Possible Opportunities and Future Research Directions

CNHs with hydrophilic properties (CNHox or holey CHNs) seem to be viable solutions as a sensing layer within resistive RH sensors design due to specific outstanding properties:

- *The absence of metallic particles as impurities* - Synthesis of the CNHs is conducted in the absence of metal catalyst [54].
- *High Surface Area* - CNHox possesses a large specific surface area (1,300–1,400 m^2/g BET), providing more sites for the adsorption of water, which increases its RH sensitivity [79].
- *Tunable Surface Chemistry* – The versatile hydrophilization of CNHs (through oxidation in solution or plasma treatment) allows for the optimization of the response of the sensor to different RH levels [54].
- *Good Electrical Conductivity* - CNHox retains good electrical conductivity even after hydrophilization, which is a key feature for resistive RH sensors. The interaction of water molecules with the CNHox surface can modify the electrical resistance of the sensing film, allowing for accurate RH monitoring [63].
- *RT Operation* - CNHox-based sensors can operate at RT, which is an advantage for manufacturing ultralow-power resistive sensors [93–95].
- *Excellent Linearity and Stability* - CNHox-based RH sensors have demonstrated excellent linearity in their response across a wide range of RH levels, and they have also shown good stability over time [83].
- *Rapid Response and Recovery Times* - The large surface area and tunable surface chemistry of CNHox contribute to obtaining fast response and recovery time [84].
- *Compatibility with other materials* - CNHox can be easily incorporated into nanocomposites or nanohybrids with different materials, like polymers (e.g. PVP, PEG-PPG-PEG), carbonic materials (GO), metal oxides (e.g., TiO_2, ZnO, SnO_2), further enhancing their sensing properties and enabling the development of RH sensors [51]
- *Potential for Flexible and Wearable Sensors* - The ability to create thin films and dispersions makes CNHox suitable for integration into flexible and wearable sensors, expanding the possible applications of RH sensors [54].

Despite the above properties, CNHs are used less than other nanocarbonic materials, such as CNTs, GO, and reduced GO, in RH monitoring. The statement is valid not only for RH sensors but also for gas sensors in general. The question is: Why are CNHs not as popular as other carbon allotropes?

A possible answer to that question is that, during their synthesis, CNHs tend to aggregate into spherical clusters, making it difficult to disperse them individually and create a homogeneous sensing layer. For many years, this was the major limitation in the chemistry of CNHs. Recently, this drawback was overcome by employing a new technique for separating the clusters into distinct nanohorns [54]. Another possible answer is that the low symmetry of CNHs reduces the number of

 doi:10.20944/preprints202507.1413.v1

predictive simulations. For these reasons, CNHs are less understood and used than other nanocarbonic materials [54].

Thus, several refined computational techniques, such as molecular dynamics (MD) and Monte Carlo (MC) simulations, and density functional theory (DFT) calculations, could offer more opportunities related to achieving an optimal level of hydrophilicity or proper functionalization.

We believe that carbon nanohorns hold significant future potential and will be utilized in an increasing number of applications, particularly in gas sensing, biomedicine, and energy storage.

8. Conclusions

The paper introduces and analyzes recent progress on resistive RT RH sensors based on CNHs, operating above the percolation threshold in the dielectric matrix. Several methods to synthesize CNHs and strategies for their hydrophilization, as well as the most important physical, chemical, and electronic properties of CNHs, were discussed in the first two sections of this review. The design of RH resistive sensors using CNHs-based materials as sensing films, as well as the synthesis and performance of several CNHs-based sensing materials in resistive RH monitoring, within the context of resistive sensor design, are presented in the following two parts of this review. Pristine and functionalized CNHs, nanocomposites including CHNs and different hydrophilic polymers (PVP, PEG-PPG-PEG) or other nanocarbonic materials (GO), nanohybrids comprising CNHs and several metal oxide semiconductors (SnO_2, TiO_2, ZnO) or hygroscopic inorganic salt (KCl) were presented and compared in terms of linearity, sensitivity, response time, and recovery time.

The fifth part of the review presented several sensing mechanisms suitable for explaining RH detection when using CNHs-based sensing layers in resistive structures. In the sixth part of the review, the authors listed the key properties that recommend CNHs as sensing layers in resistive RH detection. At the same time, the paper discusses why, for the time being, compared to graphene, GO, reduced GO, SWCNTs, and MWCNTs, CNHs are less frequently used in resistive RH detection.

Given the above rationale, one can conclude that CNHs hold huge future potential and will eventually be used in an increasing number of applications, especially in gas sensing, biomedicine (drug delivery), and energy storage (supercapacitors, batteries).

Author Contributions: Conceptualization, B.C.S.; methodology, B.C.S., M.B.(Marius Bumbac), and N.D.; validation, B.C.S., O.B., M.B.(Marius Bumbac); formal analysis, B.C.S., O.B., M.B. (Marius Bumbac), M.B. (Mihai Brezeanu), and C.C.; investigation, O.B., N.D., and C.C.; resources, B.C.S., and O.B.,; data curation, X.X.; writing—original draft preparation, B.C.S., O.B., M.B. (Marius Bumbac), M.B. (Mihai Brezeanu), U.M.G., V.D., M.R.S. and C.C.; writing—review and editing, all authors; visualization, B.C.S., O.B., M.B. (Marius Bumbac), M.B. (Mihai Brezeanu), and C.C.; supervision, B.C.S., O.B., M.B. (Marius Bumbac); project administration, B.C.S., O.B.; funding acquisition, B.C.S., O.B.. All authors have read and agreed to the published version of the manuscript.

Funding: The IMT authors acknowledge the funding received through the "National Platform for Semiconductor Technologies" project (G 2024 – 85828 / 390008 / 27.11.2024, SMIS code 304244), co-funded by the European Regional Development Fund under the Program for Intelligent Growth, Digitization, and Financial Instruments.

Conflicts of Interest: The authors declare no conflicts of interest

Abbreviations

The following abbreviations are used in this manuscript:

CNHs	Carbon nanohorns
CNHs-F	Fluorinated carbon nanohorns
CNHox	Oxidized carbon nanohorns
CNHox-F	Oxi fluorinated carbon nanohorns
CNCs	Carbon nano coils
CNCs	Carbon nano tubes

 doi:10.20944/preprints202507.1413.v1

GO	Graphene oxide
IDT	Interdigitated
LCP	Liquid crystal polymer
PDAC	Poly(diallyldimethylammonium chloride)
PEG	Poly(ethylene glycol)
PEG-PPG-PEG	Poly(ethylene glycol)-block-poly(propylene glycol)-block-poly(ethylene glycol)
PET	Polyethylene terephthalate
PPG	propylene glycol
PVA	Polyvinyl Alcohol
PVP	Polyvinylpyrrolidone
PTFE	Polytetrafluoroethylene
MWCNTs	Multi-walled carbon nanotubes
RH	Relative humidity
SWCNTs	Single-walled carbon nanotubes
SWNHs	Single-walled nanohorns
SDC	Shellac-derived carbon

References

1. Kuzubasoglu, B.A. Recent studies on the humidity sensor: A mini review. *ACS Appl. Electron. Mater.* **2022**, *4*, 4797–4807.
2. Arundel, A.V.; Sterling, E.M.; Biggin, J.H.; Sterling, T.D. Indirect health effects of relative humidity in indoor environments. *Environ. Health Perspect.* **1986**, *65*, 351–361.
3. Davis, R.E.; McGregor, G.R.; Enfield, K.B. Humidity: A review and primer on atmospheric moisture and human health. *Environ. Res.* **2016**, *144*, 106–116.
4. Wolkoff, P. Indoor air humidity, air quality, and health–An overview. *Int. J. Hyg. Environ. Health* **2018**, *221*, 376–390.
5. Barmpakos, D.; Kaltsas, G. A review on humidity, temperature, and strain printed sensors—Current trends and future perspectives. *Sensors* **2021**, *21*, 739.
6. Alam, N.; Abid; Islam, S.S. Advancements in trace and low humidity sensors technologies using nanomaterials: A review. *ACS Appl. Nano Mater.* **2024**, *7*, 13836–13864.
7. Huang, C.; Jiang, M.; Liu, F. Recent progress on environmentally friendly humidity sensor: A mini review. *ACS Appl. Electron. Mater.* **2023**, *5*, 4067–4079.
8. Sajid, M.; Khattak, Z.J.; Rahman, K.; Hassan, G.; Choi, K.H. Progress and future of relative humidity sensors: A review from materials perspective. *Bull. Mater. Sci.* **2022**, *45*, 238.
9. Korotcenkov, G.; Simonenko, N.P.; Simonenko, E.P.; Sysoev, V.V.; Brinzari, V. Based humidity sensors as promising flexible devices, state of the art, part 2: Humidity-sensor performances. *Nanomaterials* **2023**, *13*, 1381.
10. Lee, C.Y.; Lee, G.B. Humidity sensors: A review. *Sens. Lett.* **2005**, *3*, 1–15.
11. Okcan, B.; Akin, T. A thermal conductivity-based humidity sensor in a standard CMOS process. In *Proceedings of the 17th IEEE International Conference on Micro Electro Mechanical Systems (MEMS)*, Maastricht, The Netherlands, 25–29 January 2004; IEEE: New York, NY, USA, 2004; pp. 552–555.
12. Atalay, S.; Izgi, T.; Kolat, V.S.; Erdemoglu, S.; Inan, O.O. Magnetoelastic humidity sensors with TiO2 nanotube sensing layers. *Sensors* **2020**, *20*, 425.
13. Zhang, M.; Duan, Z.; Zhang, B.; Yuan, Z.; Zhao, Q.; Jiang, Y.; Tai, H. Electrochemical humidity sensor enabled self-powered wireless humidity detection system. *Nano Energy* **2023**, *115*, 108745.
14. Wu, T.T.; Chen, Y.Y.; Chou, T.H. A high sensitivity nanomaterial-based SAW humidity sensor. *J. Phys. D Appl. Phys.* **2008**, *41*, 085101.
15. Ashley, G.M.; Kirby, P.B.; Butler, T.P.; Whatmore, R.; Luo, J.K. Chemically sensitized thin-film bulk acoustic wave resonators as humidity sensors. *J. Electrochem. Soc.* **2010**, *157*, J419.
16. Ascorbe, J.; Corres, J.M.; Arregui, F.J.; Matias, I.R. Recent developments in fiber optics humidity sensors. *Sensors* **2017**, *17*, 893.
17. Ragazzini, I.; Castagnoli, R.; Gualandi, I.; Cassani, M.C.; Nanni, D.; Gambassi, F.; Ballarin, B. A resistive sensor for humidity detection based on cellulose/polyaniline. *RSC Adv.* **2022**, *12*, 28217–28226.

 doi:10.20944/preprints202507.1413.v1

18. Hussain, M.; Hasnain, S.; Khan, N.A.; Bano, S.; Zuhra, F.; Ali, M.; Ali, A. Design and fabrication of a fast response resistive-type humidity sensor using polypyrrole (ppy) polymer thin film structures. *Polymers* **2021**, *13*, 3019.
19. Packirisamy, M.; Stiharu, I.; Li, X.; Rinaldi, G. A polyimide based resistive humidity sensor. *Sens. Rev.* **2005**, *25*, 271–276.
20. Demir, R.; Okur, S.; Seker, M. Electrical characterization of CdS nanoparticles for humidity sensing applications. *Ind. Eng. Chem. Res.* **2012**, *51*, 3309–3313.
21. Chang, S.P.; Chang, S.J.; Lu, C.Y.; Li, M.J.; Hsu, C.L.; Chiou, Y.Z.; Chen, I.C. A ZnO nanowire-based humidity sensor. *Superlattices Microstruct.* **2010**, *47*, 772–778.
22. Kumar, A.; Kumari, P.; Kumar, M.S.; Gupta, G.; Shivagan, D.D.; Bapna, K. SnO2 nanostructured thin film as humidity sensor and its application in breath monitoring. *Ceram. Int.* **2023**, *49*, 24911–24921.
23. Dai, J.; Zhao, H.; Lin, X.; Liu, S.; Liu, Y.; Liu, X.; Zhang, T. Ultrafast response polyelectrolyte humidity sensor for respiration monitoring. *ACS Appl. Mater. Interfaces* **2019**, *11*, 6483–6490.
24. Tambwe, K.; Ross, N.; Baker, P.; Bui, T.T.; Goubard, F. Humidity sensing applications of lead-free halide perovskite nanomaterials. *Materials* **2022**, *15*, 4146.
25. Tulliani, J.M.; Inserra, B.; Ziegler, D. Carbon-based materials for humidity sensing: A short review. *Micromachines* **2019**, *10*, 232.
26. Smith, A.D.; Elgammal, K.; Niklaus, F.; Delin, A.; Fischer, A.C.; Vaziri, S.; Lemme, M.C. Resistive graphene humidity sensors with rapid and direct electrical readout. *Nanoscale* **2015**, *7*, 19099–19109.
27. Saqib, M.; Ali Khan, S.; Mutee Ur Rehman, H.M.; Yang, Y.; Kim, S.; Rehman, M.M.; Young Kim, W. High-performance humidity sensor based on the graphene flower/zinc oxide composite. *Nanomaterials* **2021**, *11*, 242.
28. Popov, V.I.; Kotin, I.A.; Nebogatikova, N.A.; Smagulova, S.A.; Antonova, I.V. Graphene-PEDOT:PSS humidity sensors for high sensitive, low-cost, highly-reliable, flexible, and printed electronics. *Materials* **2019**, *12*, 3477.
29. Ghosh, S.; Ghosh, R.; Guha, P.K.; Bhattacharyya, T.K. Humidity sensor based on high proton conductivity of graphene oxide. *IEEE Trans. Nanotechnol.* **2015**, *14*, 931–937.
30. Noh, W.; Go, Y.; An, H. Reduced graphene oxide/polyelectrolyte multilayers for fast resistive humidity sensing. *Sensors* **2023**, *23*, 1977.
31. Zhang, X.; Maddipatla, D.; Bose, A.K.; Hajian, S.; Narakathu, B.B.; Williams, J.D.; Atashbar, M.Z. Printed carbon nanotubes-based flexible resistive humidity sensor. *IEEE Sens. J.* **2020**, *20*, 12592–12601.
32. Pan, X.; Xue, Q.; Zhang, J.; Guo, Q.; Jin, Y.; Lu, W.; Ling, C. Effective enhancement of humidity sensing characteristics of novel thermally treated MWCNTs/Polyvinylpyrrolidone film caused by interfacial effect. *Adv. Mater. Interfaces* **2016**, *3*, 1600153.
33. Serban, B.C.; Dumbravescu, N.; Buiu, O.; Bumbac, M.; Brezeanu, M.; Pachiu, C.; Tucureanu, V. Carbon Nano-Onions-Based Matrix Nanocomposite as Sensing Film for Resistive Humidity Sensor. *Rom. J. Inf. Sci. Technol.* **2025**, *28*, 77–88.
34. Serban, B.C.; Dumbravescu, N.; Buiu, O.; Bumbac, M.; Dumbravescu, C.; Brezeanu, M.; Brincoveanu, O. Carbon Nano-Onions–Polyvinyl Alcohol Nanocomposite for Resistive Monitoring of Relative Humidity. *Sensors* **2025**, *25*, 3047.
35. Yoo, K.P.; Lim, L.T.; Min, N.K.; Lee, M.J.; Lee, C.J.; Park, C.W. Novel resistive-type humidity sensor based on multiwall carbon nanotube/polyimide composite films. *Sens. Actuators B Chem.* **2010**, *145*, 120–125.
36. Epeloa, J.; Repetto, C.E.; Gómez, B.J.; Nachez, L.; Dobry, A. Resistivity humidity sensors based on hydrogenated amorphous carbon films. *Mater. Res. Express* **2018**, *6*, 025604.
37. Zhang, W.; Huang, Y.; Lin, S.; Xiao, H.; Huang, C.; Yu, W.; Xia, C. A thin film resistive humidity sensor based on polymer and carbon black nanoparticle composites. *Meas. Sci. Technol.* **2023**, *35*, 025140.
38. Joshi, S.R.; Kim, B.; Kim, S.K.; Song, W.; Park, K.; Kim, G.H.; Shin, H. Low-cost and fast-response resistive humidity sensor comprising biopolymer-derived carbon thin film and carbon microelectrodes. *J. Electrochem. Soc.* **2020**, *167*, 147511.
39. Wu, J.; Sun, Y.M.; Wu, Z.; Li, X.; Wang, N.; Tao, K.; Wang, G.P. Carbon nanocoil-based fast-response and flexible humidity sensor for multifunctional applications. *ACS Appl. Mater. Interfaces* **2019**, *11*, 4242–4251.

 doi:10.20944/preprints202507.1413.v1

40. Meng, J.; Liu, T.; Meng, C.; Lu, Z.; Li, J. Porous carbon nanofibres with humidity sensing potential. *Microporous Mesoporous Mater.* **2023**, *359*, 112663.
41. Chu, J.; Peng, X.; Feng, P.; Sheng, Y.; Zhang, J. Study of humidity sensors based on nanostructured carbon films produced by physical vapor deposition. *Sens. Actuators B Chem.* **2013**, *178*, 508–513.
42. Zhang, X.; Ming, H.; Liu, R.; Han, X.; Kang, Z.; Liu, Y.; Zhang, Y. Highly sensitive humidity sensing properties of carbon quantum dots films. *Mater. Res. Bull.* **2013**, *48*, 790–794.
43. Afify, A.S.; Ahmad, S.; Khushnood, R.A.; Jagdale, P.; Tulliani, J.-M. Elaboration and characterization of novel humidity sensor based on micro-carbonized bamboo particles. *Sens. Actuators B Chem.* **2017**, *239*, 1251–1256.
44. Ziegler, D.; Palmero, P.; Giorcelli, M.; Tagliaferro, A.; Tulliani, J.M. Biochars as innovative humidity sensing materials. *Chemosensors* **2017**, *5*, 35.
45. Ruiz, V.; Fernández, I.; Carrasco, P.; Cabañero, G.; Grande, H.J.; Herrán, J. Graphene quantum dots as a novel sensing material for low-cost resistive and fast-response humidity sensors. *Sens. Actuators B Chem.* **2015**, *218*, 73–77.
46. Ionete, E.I.; Spiridon, S.I.; Monea, B.F.; Ebrasu-Ion, D.; Vaseashta, A. SWCNT-Pt-P2O5-Based Sensor for Humidity Measurements. *IEEE Sens. J.* **2016**, *16*, 7593–7599.
47. Zhou, G.; Byun, J.H.; Oh, Y.; Jung, B.M.; Cha, H.J.; Seong, D.G.; Chou, T.W. Highly sensitive wearable textile-based humidity sensor made of high-strength, single-walled carbon nanotube/poly(vinyl alcohol) filaments. *ACS Appl. Mater. Interfaces* **2017**, *9*, 4788–4797.
48. Dai, H.; Feng, N.; Li, J.; Zhang, J.; Li, W. Chemiresistive humidity sensor based on chitosan/zinc oxide/single-walled carbon nanotube composite film. *Sens. Actuators B Chem.* **2019**, *283*, 786–792.
49. Qin, J.; Yang, X.; Shen, C.; Chang, Y.; Deng, Y.; Zhang, Z.; Shan, C. Carbon nanodot-based humidity sensor for self-powered respiratory monitoring. *Nano Energy* **2022**, *101*, 107549.
50. Liu, X.; Ying, Y.; Ping, J. Structure, synthesis, and sensing applications of single-walled carbon nanohorns. *Biosens. Bioelectron.* **2020**, *167*, 112495.
51. Serban, B.C.; Bumbac, M.; Buiu, O.; Cobianu, C.; Brezeanu, M.; Nicolescu, C. Carbon nanohorns and their nanocomposites: Synthesis, properties, and applications. A concise review. *Ann. Acad. Rom. Sci. Ser. Math. Appl.* **2018**, *11*, 5–18.
52. Zhu, S.; Xu, G. Single-walled carbon nanohorns and their applications. *Nanoscale* **2010**, *2*, 2538–2549.
53. Liu, X.; Ying, Y.; Ping, J. Structure, synthesis, and sensing applications of single-walled carbon nanohorns. *Biosens. Bioelectron.* **2020**, *167*, 112495.
54. Karousis, N.; Suarez-Martinez, I.; Ewels, C.P.; Tagmatarchis, N. Structure, properties, functionalization, and applications of carbon nanohorns. *Chem. Rev.* **2016**, *116*, 4850–4883.
55. Li, N.; Wang, Z.; Zhao, K.; Shi, Z.; Gu, Z.; Xu, S. Synthesis of single-wall carbon nanohorns by arc-discharge in air and their formation mechanism. *Carbon* **2010**, *48*, 1580–1585.
56. Gattia, D.M.; Antisari, M.V.; Marazzi, R. AC arc discharge synthesis of single-walled nanohorns and highly convoluted graphene sheets. *Nanotechnology* **2007**, *18*, 255604.
57. Berkmans, J.; Jagannatham, M.; Reddy, R.; Haridoss, P. Synthesis of thin bundled single-walled carbon nanotubes and nanohorn hybrids by arc discharge technique in open air atmosphere. *Diam. Relat. Mater.* **2015**, *55*, 12–15.
58. Wang, H.; Chhowalla, M.; Sano, N.; Jia, S.; Amaratunga, G.A.J. Large-scale synthesis of single-walled carbon nanohorns by submerged arc. *Nanotechnology* **2004**, *15*, 546.
59. Yuge, R.; Yudasaka, M.; Toyama, K.; Yamaguchi, T.; Iijima, S.; Manako, T. Buffer gas optimization in CO2 laser ablation for structure control of single-wall carbon nanohorn aggregates. *Carbon* **2012**, *50*, 1925–1933.
60. Schiavon, M. Device and Method for Production of Carbon Nanotubes, Fullerene and their Derivatives. U.S. Patent 7,125,525; EP 1428794, Filed 2003, Granted 2006.
61. Casteignau, F.; Aissou, T.; Allard, C.; Ricolleau, C.; Veilleux, J.; Martel, R.; Braidy, N. Synthesis of carbon nanohorns by inductively coupled plasma. *Plasma Chem. Plasma Process.* **2022**, *42*, 465–481.
62. Cioffi, C.; Campidelli, S.; Sooambar, C.; Marcaccio, M.; Marcolongo, G.; Meneghetti, M.; Prato, M. Synthesis, characterization, and photoinduced electron transfer in functionalized single-wall carbon nanohorns. *J. Am. Chem. Soc.* **2007**, *129*, 3938–3945.

 doi:10.20944/preprints202507.1413.v1

63. Arti, N.; Alam, N.; Ansari, J.R. Nanostructures and Fascinating Properties of Carbon Nanohorns. In *Handbook of Functionalized Carbon Nanostructures: From Synthesis Methods to Applications*; Springer International Publishing: Cham, Switzerland, 2024; pp. 351–389.
64. Serban, B.C.; Buiu, O.; Marinescu, M.R. Resistive humidity sensor based on fluorinated nanocarbon materials. *RO137256A2*, 2023.
65. Serban, B.C.; Buiu, O.; Marinescu, M.R. Oxy-fluoro-nanocarbon sensitive layers for resistive detection of humidity. *RO137257A2*, 2023.
66. Kumar, P.S.; Kumar, K.S.; Geethan, K.A.; Santhosh, D. Properties and Potential Applications of Carbon Nano Horns Over Carbon Nano Tubes as a Nano Fluid—A Review. In *IOP Conference Series: Materials Science and Engineering*; IOP Publishing: 2021; Volume 1130, p. 012008.
67. Yuge, R.; Nihey, F.; Toyama, K.; Yudasaka, M. Preparation, electrical properties, and supercapacitor applications of fibrous aggregates of single-walled carbon nanohorns. *Carbon* **2018**, *138*, 379–383.
68. Jung, H.J.; Kim, Y.J.; Han, J.H.; Yudasaka, M.; Iijima, S.; Kanoh, H.; Yang, C.M. Thermal-treatment-induced enhancement in effective surface area of single-walled carbon nanohorns for supercapacitor application. *J. Phys. Chem. C* **2013**, *117*, 25877–25883.
69. Utsumi, S.; Miyawaki, J.; Tanaka, H.; Hattori, Y.; Itoi, T.; Ichikuni, N.; Kaneko, K. Opening mechanism of internal nanoporosity of single-wall carbon nanohorn. *J. Phys. Chem. B* **2005**, *109*, 14319–14324.
70. Zambano, A.J.; Talapatra, S.; Lafdi, K.; Aziz, M.T.; McMillin, W.; Shaughnessy, G.; Takahashi, K. Adsorbate binding energy and adsorption capacity of xenon on carbon nanohorns. *Nanotechnology* **2002**, *13*, 201.
71. Nisha, J.A.; Yudasaka, M.; Bandow, S.; Kokai, F.; Takahashi, K.; Iijima, S. Adsorption and catalytic properties of single-wall carbon nanohorns. *Chem. Phys. Lett.* **2000**, *328*, 381–386.
72. Hou, S.; Xie, Z.; Zhang, D.; Yang, B.; Lei, Y.; Liang, F. High-purity graphene and carbon nanohorns prepared by base-acid treated waste tires carbon via direct current arc plasma. *Environ. Res.* **2023**, *238*, 117071.
73. Peng, H.; Xie, Z.; Lu, S.; Zhang, D.; Yang, B.; Liang, F. Dual-functionality composites of polyaniline-coated oxidized carbon nanohorns: Efficient wave absorption and enhanced corrosion resistance. *Chin. Chem. Lett.* **2025**, *110818*.
74. Zhu, S.; Xu, G. Carbon nanohorns and their biomedical applications. *Nanotechnologies for the Life Sciences* **2012**, *9*.
75. Pandit, J.; Alam, M.S.; Javed, M.N.; Waziri, A.; Imam, S.S. Emerging roles of carbon nanohorns as sustainable nanomaterials in sensor, catalyst, and biomedical applications. In *Handbook of Green and Sustainable Nanotechnology: Fundamentals, Developments and Applications*; Springer International Publishing: Cham, Switzerland, 2023; pp. 1721–1747.
76. Serban, B.C.; Cobianu, C.; Dumbravescu, N.; Buiu, O.; Bumbac, M.; Nicolescu, C.M.; Serbanescu, M. Electrical percolation threshold and size effects in polyvinylpyrrolidone-oxidized single-wall carbon nanohorn nanocomposite: The impact for relative humidity resistive sensors design. *Sensors* **2021**, *21*, 1435.
77. Serban, B.C.; Cobianu, C.; Dumbrăvescu, N.; Buiu, O.; Avramescu, V.; Bumbac, M.; Brezeanu, M. Electrical percolation threshold in oxidized single-wall carbon nanohorn-polyvinylpyrrolidone nanocomposite: A possible application for high sensitivity resistive humidity sensor. In *2020 International Semiconductor Conference (CAS)*, Sinaia, Romania, 7–9 October 2020; IEEE: New York, NY, USA, 2020; pp. 239–242.
78. Pagona, G.; Sandanayaka, A.S.; Araki, Y.; Fan, J.; Tagmatarchis, N.; Charalambidis, G.; Ito, O. Covalent functionalization of carbon nanohorns with porphyrins: Nanohybrid formation and photoinduced electron and energy transfer. *Adv. Funct. Mater.* **2007**, *17*, 1705–1711.
79. Serban, B.C.; Buiu, O.; Dumbravescu, N.; Cobianu, C.; Avramescu, V.; Brezeanu, M.; Nicolescu, C.M. Oxidized carbon nanohorns as novel sensing layer for resistive humidity sensor. *Acta Chim. Slov.* **2020**, *67*, 2.
80. Selvam, K.P.; Nakagawa, T.; Marui, T.; Inoue, H.; Nishikawa, T.; Hayashi, Y. Synthesis of solvent-free conductive and flexible cellulose–carbon nanohorn sheets and their application as a water vapor sensor. *Mater. Res. Express* **2020**, *7*, 056402.

 doi:10.20944/preprints202507.1413.v1

81. Șerban, B.C.; Buiu, O.; Cobianu, C.; Avramescu, V.; Pachiu, C.; Ionescu, O.; Marinescu, M.R. Chemiresistive humidity sensor based on carbon nanocomposites. *RO 134261 A2*, Priority: 29 November 2018; Official Bulletin of Industrial Property—Patents Section, 30 June 2020.
82. Șerban, B.C.; Cobianu, C.; Dumbrăvescu, N.; Buiu, O.; Oxidized Carbon Nanohorns and Their Nanocompozites as Sensing Layers for Chemiresistive Relative Humidity Sensor, Spring Scientific Conference of the Romanian Academy of Scientists, April 4-6, 2019, Bucharest, pg.34.
83. Serban, B.C.; Cobianu, C.; Dumbrăvescu, N.; Buiu, O.; Avramescu, V.; Brezeanu, M.; Nicolescu, C.M.; Serbanescu, M. Oxidized carbon nanohorn-hydrophilic polymer nanocomposite as the resistive sensing layer for relative humidity. *Anal. Lett.* **2021**, *54*, 527–540.
84. Serban, B.C.; Buiu, O.; Bumbac, M.; Dumbravescu, N.; Pachiu, C.; Brezeanu, M.; Cobianu, C. Ternary nanocomposites based on oxidized carbon nanohorns as sensing layers for room temperature resistive humidity sensing. *Materials* **2021**, *14*, 2705.
85. Șerban, B.C.; Buiu, O.; Cobianu, C.; Avramescu, V.; Dumbrăvescu, N.; Brezeanu, M.; Marinescu, M.R. Ternary carbon-based nanocomposite as sensing layer for resistive humidity sensor. In *Proceedings of the 29th International Semiconductor Conference*, Sinaia, Romania, 7–9 October 2019; MDPI: Basel, Switzerland, 2019; Volume 1, p. 114.
86. Serban, B.C.; Dumbrăvescu, N.; Buiu, O.; Bumbac, M.; Pachiu, C.; Brezeanu, M.; Cobianu, C. Carbon Nanohorns-PVP Nanocomposite as Sensing Layer for Resistive Humidity Monitoring: Preliminary Results. In *2024 International Semiconductor Conference (CAS)*, Sinaia, Romania, 9–11 October 2024; IEEE: New York, NY, USA, 2024; pp. 39–42.
87. Bogdan-Catalin Serban; Octavian Buiu; Nicolae Dumbrăvescu; Mihai Brezeanu; Marius Bumbac; Cristina Mihaela Nicolescu; Vlad Diaconescu. Pristine carbon nanohorns-polyvinyl pyrrolidone as sensing film for relative humidity detection. *7th International Conference on Emerging Technologies in Materials Engineering*, Bucharest, Romania, 30–31 October 2024; Book of Abstracts, p. 168.
88. Shakeel, A.; Rizwan, K.; Farooq, U.; Iqbal, S.; Altaf, A.A. Advanced polymeric/inorganic nanohybrids: An integrated platform for gas sensing applications. *Chemosphere* **2022**, *294*, 133772.
89. Verma, A.; Yadav, D.; Natesan, S.; Gupta, M.; Yadav, B.C.; Mishra, Y.K. Advancements in nanohybrid material-based acetone gas sensors relevant to diabetes diagnosis: A comprehensive review. *Microchem. J.* **2024**, *110713*.
90. Jiang, T.; Wang, Z.; Li, Z.; Wang, W.; Xu, X.; Liu, X.; Wang, C. Synergic effect within n-type inorganic–p-type organic nano-hybrids in gas sensors. *J. Mater. Chem. C* **2013**, *1*, 3017–3025.
91. Zegebreal, L.T.; Tegegne, N.A.; Hone, F.G. Recent progress in hybrid conducting polymers and metal oxide nanocomposite for room-temperature gas sensor applications: A review. *Sens. Actuators A Phys.* **2023**, *359*, 114472.
92. Serban, B.C.; Dumbrăvescu, N.; Buiu, O.; Bumbac, M.; Brezeanu, M.; Cobianu, C.; Nicolescu, C.M. Oxidized carbon nanohorns/KCl/PVP nanohybrid as sensing layer for chemiresistive humidity sensor. In *2023 International Semiconductor Conference (CAS)*, Sinaia, Romania, 11–13 October 2023; IEEE: New York, NY, USA, 2023; pp. 75–78.
93. Serban, B.C.; Buiu, O.; Bumbac, M.; Dumbravescu, N.; Pachiu, C.; Brezeanu, M.; Cobianu, C. Ternary Holey Carbon Nanohorn/Potassium Chloride/Polyvinylpyrrolidone Nanohybrid as Sensing Film for Resistive Humidity Sensor. *Coatings* **2024**, *14*, 517.
94. Bogdan-Catalin Șerban; Octavian Buiu; Nicolae Dumbrăvescu; Viorel Avramescu; Mihai Brezeanu; Maria-Roxana Marinescu; Marius Bumbac; Cristina Nicolescu. Hydrophilic oxidized carbon nanohorns/PVP/KCl nanohybrid for chemiresistive humidity sensor. *14th International Conference on Physics of Advanced Materials (ICPAM-14)*, Dubrovnik, Croatia, 8–15 September 2022; Book of Abstracts, pp. 262–263.
95. Serban, B.C.; Buiu, O.; Bumbac, M.; Dumbravescu, N.; Avramescu, V.; Brezeanu, M.; Comanescu, F. Ternary Holey Carbon Nanohorns/TiO2/PVP nanohybrids as sensing films for resistive humidity sensors. *Coatings* **2021**, *11*, 1065.
96. Serban, B.C.; Buiu, O.; Bumbac, M.; Marinescu, R.; Dumbravescu, N.; Avramescu, V.; Comanescu, F. Ternary oxidized carbon nanohorns/TiO2/PVP nanohybrid as sensitive layer for chemoresistive humidity sensor. *Chem. Proc.* **2021**, *5*, 12.

 doi:10.20944/preprints202507.1413.v1

97. Ohsaka, T.; Izumi, F.; Fujiki, Y. Raman spectrum of anatase, TiO2. *J. Raman Spectrosc.* **1978**, *7*, 321–324.
98. Choi, H.C.; Jung, Y.M.; Kim, S.B. Size effects in the Raman spectra of TiO2 nanoparticles. *Vib. Spectrosc.* **2005**, *37*, 33–38.
99. Mathpal, M.C.; Tripathi, A.K.; Singh, M.K.; Gairola, S.P.; Pandey, S.N.; Agarwal, A. Effect of annealing temperature on Raman spectra of TiO2 nanoparticles. *Chem. Phys. Lett.* **2013**, *555*, 182–186.
100. Serban, B.C.; Dumbrăvescu, N.; Buiu, O.; Bumbac, M.; Brezeanu, M.; Cobianu, C.; Nicolescu, C.M. Ternary holey carbon-based nanohybrid for resistive relative humidity sensor. In *2023 International Semiconductor Conference (CAS)*, Sinaia, Romania, 11–13 October 2023; IEEE: New York, NY, USA, 2023; pp. 25–28.
101. Serban, B.C.; Cobianu, C.; Buiu, O.; Bumbac, M.; Dumbravescu, N.; Avramescu, V.; Comanescu, F.C. Quaternary holey carbon nanohorns/SnO2/ZnO/PVP nano-hybrid as sensing element for resistive-type humidity sensor. *Coatings* **2021**, *11*, 1307.
102. Serban, B.C.; Cobianu, C.; Buiu, O.; Bumbac, M.; Dumbravescu, N.; Avramescu, V.; Comanescu, F. Quaternary Oxidized Carbon Nanohorns—Based Nanohybrid as Sensing Coating for Room Temperature Resistive Humidity Monitoring. *Coatings* **2021**, *11*, 530.
103. Zieleniewska, A.; Lodermeyer, F.; Prato, M.; Rumbles, G.; Guldi, D.M.; Blackburn, J.L. Elucidating the electronic properties of single-wall carbon nanohorns. *J. Mater. Chem. C* **2022**, *10*, 5783–5786.
104. Uceta, H.; Cabrera-Espinoza, A.; Barrejón, M.; Sánchez, J.G.; Gutierrez-Fernandez, E.; Kosta, I.; Delgado, J.L. p-Type Functionalized Carbon Nanohorns and Nanotubes in Perovskite Solar Cells. *ACS Appl. Mater. Interfaces* **2023**, *15*, 45212–45228.
105. Zhang, D.; Tong, J.; Xia, B. Humidity-sensing properties of chemically reduced graphene oxide/polymer nanocomposite film sensor based on layer-by-layer nano self-assembly. *Sens. Actuators B Chem.* **2014**, *197*, 66–72.
106. Pearson, R.G. Hard and soft acids and bases, HSAB, part 1: Fundamental principles. *J. Chem. Educ.* **1968**, *45*, 581.
107. Pearson, R.G. Hard and soft acids and bases, HSAB, part II: Underlying theories. *J. Chem. Educ.* **1968**, *45*, 643.
108. Pearson, R.G. The HSAB principle—more quantitative aspects. *Inorg. Chim. Acta* **1995**, *240*, 93–98.
109. Ayers, P.W.; Parr, R.G.; Pearson, R.G. Elucidating the hard/soft acid/base principle: A perspective based on half-reactions. *J. Chem. Phys.* **2006**, *124*, 194107.
110. Serban, B.; Kumar, A.S.; Costea, S.; Mihaila, M.; Buiu, O.; Brezeanu, M.; Cobianu, C. Polymer-amino carbon nanotube nanocomposites for surface acoustic wave CO2 detection. *Rom. J. Inf. Sci. Technol.* **2009**, *12*, 376–384.
111. Serban, B.C.; Brezeanu, M.; Cobianu, C.; Costea, S.; Buiu, O.; Stratulat, A.; Varachiu, N. Materials selection for gas sensing: An HSAB perspective. In *2014 International Semiconductor Conference (CAS)*, Sinaia, Romania, 13–15 October 2014; IEEE: New York, NY, USA, 2014; pp. 21–30.
112. Serban, B.; Kumar, A.S.; Cobianu, C.; Buiu, O.; Costea, S.; Bostan, C.; Varachiu, N. Selection of sensing materials using the Hard Soft Acid Base theory; application to Surface Acoustic Wave CO2 detection. In *CAS 2010 Proceedings (International Semiconductor Conference)*, Sinaia, Romania, 11–13 October 2010; IEEE: New York, NY, USA, 2010; Volume 1, pp. 247–250.
113. Serban, B.C.; Buiu, O.; Dumbrăvescu, N.; Brezeanu, M.; Cobianu, C.; Bumbac, M.; Nicolescu, M. Some considerations about the sensing mechanisms and electrical response of carbon nanohorns–based gas sensors. *Sci. Technol.* **2024**, *27*, 137–150.
114. Agmon, N. The Grotthuss mechanism. *Chem. Phys. Lett.* **1995**, *244*, 456–462.